the vRNA segments per se play a role in the efficient formation of infectious virions.

Recently, Liang et al. (19) confirmed that, as with the segments we studied, both ends of the coding regions of PB2, PB1, and PA vRNAs are necessary for their efficient incorporation into virions. However, in their experiments, cells were transfected with plasmids for the expression of all eight wild-type vRNA segments, together with a plasmid expressing a test vRNA that comprised a reporter gene and a portion of one of the polymerase vRNA segments. Under these conditions, a test vRNA and its parent vRNA would compete for packaging into virions. This experimental approach complicates the analysis of the reporter vRNA incorporation efficiency and confounds interpretation of the data. We therefore took an alterative approach. We studied the incorporation of the polymerase vRNA segments under conditions in which the test vRNA did not have to compete with the parental wild-type RNA for virion incorporation, i.e., by providing seven wild-type vRNA segments and a test vRNA segment. Not only do these conditions more authentically mirror virus-infected cells, but they also allowed us to ask whether the regions important for the incorporation of a particular vRNA segment into virions also affect the virion incorporation efficiencies of the other vRNA segments.

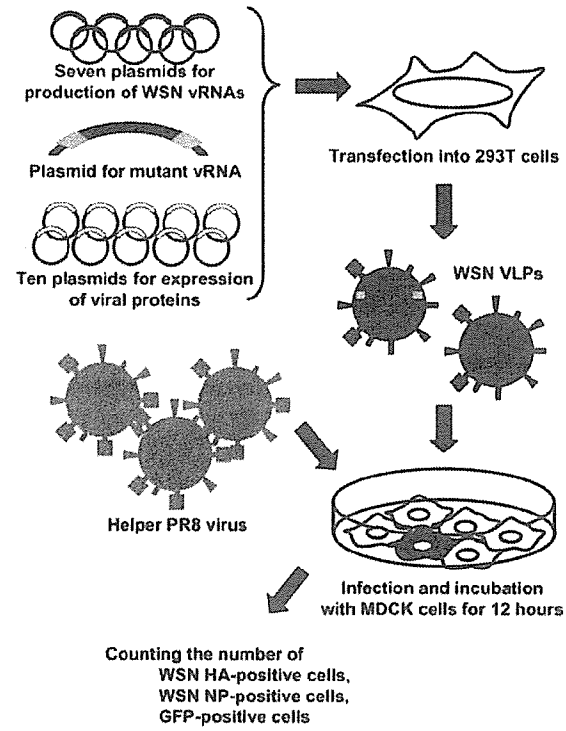

FIG. 1. Schematic representation of the system used to determine infectious virion formation and the incorporation efficiencies of test vRNA segments. 293T cells were transfected with plasmids for the production of WSN VLPs. Forty-eight hours later, the supernatants were mixed with helper PR8 virus and used to infect MDCK cells. At 12 h postinfection, the numbers of GFP- or WSN HA-positive cells were counted by flow cytometry; alternatively, the numbers of cells expressing WSN NP were determined. The number of cells expressing HA or NP was used to determine the number of infectious VLPs in the experiments presented in Table 1. The number of cells expressing GFP reflects the number of VLPs possessing a test vRNA. The incorporation efficiency of a test vRNA was determined by dividing the number of GFP-expressing cells by the sum of the number of cells expressing WSN HA and the number of GFP-expressing cells.

MATERIALS AND METHODS

Cells and viruses. 293T human embryonic kidney cells were maintained in Dulbecco's modified Eagle's medium supplemented with 10% fetal calf serum and antibiotics. Madin-Darby canine kidney (MDCK) cells were grown in minimal essential medium (MEM) containing 10% newborn calf serum and antibiotics. After infection with influenza virus, the MDCK cells were maintained in MEM containing 0.3% bovine serum albumin (BSA). A/Puerto Rico/8/34 (PR8, H1N1) viruses were propagated in MDCK cells.

Reverse genetics. Reverse genetics was performed with plasmids that contain cDNAs of the A/WSN/33 (WSN, H1N1) viral genes between the human RNA polymerase I promoter and the mouse RNA polymerase I terminator (referred to as PolI plasmids) and eukaryotic protein expression plasmids under the control of the chicken β-actin promoter (16, 23), as described previously (21). Briefly, PolI plasmids and protein expression plasmids were mixed with the transfection reagent TransIT-293 (Mirus, Madison, WI), incubated at room temperature for 15 min, and added to 10^6 293T cells cultured in Opti-MEM I (Gibco-BRL). The total volume of the supernatant was adjusted to 1 ml. Forty-eight hours later, the supernatant containing infectious virus-like particles (VLPs) was harvested. In this study, the generated particles are unable to undergo multiple cycles of replication; hence, they will be referred to as VLPs.

Construction of plasmids. Plasmid pPolIPB2(0)GFP(0) allows the synthesis of a negative-sense vRNA comprising the 3′ noncoding region of the PB2 vRNA, the complementary coding sequence of enhanced green fluorescent protein (GFP) (Clontech), and the 5′ noncoding region of the PB2 vRNA. To generate this plasmid, we amplified pPolIPB2 (a plasmid for the production of wild-type PB2 vRNA [22]) by inverse PCR (26) using the back-to-back primers PB2-0-F (5′-CACACAGGTCTCAATAATGTCGAATAGTTTAAAAACGACCTTGTT TCTAC-3′) and PB2-0-R (5′-CACACAGGTCTCACCATATTGAATATAATT GACCTGCTTTCGCT-3′), both of which contain BsaI sites. The GFP gene was amplified by PCR with BbsI-containing primers. The two PCR fragments were incubated with the respective enzymes and ligated to produce pPolIPB2(0)GFP(0). Using the same strategy, we also generated a series of constructs that contained portions of the PB2 coding regions, in addition to the noncoding regions (see Fig. 2). These mutants were named according to the lengths of the coding region(s) they contained; PB2(120)GFP(30), for example, contains the 3′ PB2 noncoding region, 120 nucleotides that correspond to the coding sequence at the 3′ end of the vRNA, the GFP coding sequence, 30 nucleotides that correspond to the coding sequence at the 5′ end of the vRNA, and the 5′ PB2 noncoding region.

Similarly, a series of PB1 and PA plasmids were produced. For the PB1 segment, a plasmid for the production of wild-type PB1 vRNA (pPolIPB1) was amplified by inverse PCR using primers that contain BsmBI sites: PB1-120-F (5′-CACACACGTCTCAATAAGTTTCCAGAGCCCGAATTG-3′) and PB1-120-R (5′-CACACACGTCTCACCATCATGGTGTATCCTGTTCCTG-3′). For the PA segment, we amplified pPolIPA, which produces wild-type PA vRNA, by inverse PCR with the following primers that contain BsmBI sites: PA-120-F (5′-CACACAGGTCTCAATAACCTGGGACCTTTGATCTTG-3′) and PA-120-R (5′-CACACAGGTCTCACCATAGTGCATATTGCTGCAAATTTGTTTG-3′). The PCR products were incubated with BsmBI and ligated with the GFP fragment to produce pPolIPB1(120)GFP(120) and pPolIPA(120)GFP(120), respectively. Deletion constructs were produced by employing the same strategy. All plasmid constructs were sequenced to ensure that unwanted mutations were not introduced by PCR.

Determination of the total number of VLPs and the number of VLPs containing test vRNAs (Fig. 1). 293T cells were transfected with a PolI plasmid transcribing a test vRNA derived from the PA, PB1, or PB2 vRNA, with plasmids for the transcription of the remaining seven vRNAs, and with plasmids for the expression of all 10 viral proteins. Forty-eight hours later, the supernatants were harvested, mixed with helper PR8 virus (multiplicity of infection, 0.1), and adsorbed to MDCK cells for 1 h at 37°C. The helper PR8 virus was included to provide functional polymerase proteins because the test vRNAs possessing the GFP gene do not encode these proteins. The MDCK cells were then washed with phosphate-buffered saline (PBS) and incubated with MEM for an additional 11 h.

Twelve hours postinfection, the numbers of cells expressing HA or NP protein or the reporter gene GFP were determined. To detect HA-positive cells, the cells were dispersed with a solution containing 0.025% trypsin and 0.02% EDTA and subsequently incubated in PBS containing 1% BSA and 0.1% sodium azide for 1 h on ice. After centrifugation, the cells were incubated for 1 h on ice with a

PB2 mutant vRNAs		Number of VLPs (/ml)	Number of VLPs possessing GFP vRNA (/ml)	Efficiency of virion incorporation
	3' 5'			
PB2(300)GFP(300)		2,799,200	1,532,400	54.7%
PB2(120)GFP(120)		1,080,800	753,600	69.7%
PB2(60)GFP(120)		1,676,800	960,000	57.3%
PB2(30)GFP(120)		1,807,200	839,200	46.4%
PB2(0)GFP(120)		1,093,600	322,400	29.5%
PB2(120)GFP(60)		1,756,800	1,132,800	64.5%
PB2(120)GFP(30)		1,068,000	549,600	51.5%
PB2(120)GFP(0)		56,000	42,400	75.7%
PB2(0)GFP(0)		28,000	0	0.0%
PB2(-)	None	19,600	-	-

FIG. 2. Schematic diagram of mutant PB2 vRNAs and their efficiencies in virion formation and virion incorporation. The numbers of VLPs and the virion incorporation efficiencies of mutant PB2 vRNAs were determined by using the numbers of WSN HA- and GFP-expressing cells as a denominator. All mutants are shown in the negative-sense orientation. Each mutant contains the GFP reading frame (green bar); 27 and 34 nucleotides of the 3′ and 5′ noncoding regions, respectively (gray bars); and coding regions of various lengths (black bars). The dotted lines represent deleted sequences of the PB2 coding region. PB2(−) indicates the omission of this vRNA (i.e., VLPs were generated using only seven vRNA segments). The results shown are representative data from six independent experiments.

monoclonal antibody (967/8) that recognizes the WSN HA protein. The anti-HA mouse monoclonal antibody (967/8) reacted with the HA protein of WSN but not that of the PR8 virus (unpublished data). The cells were washed twice with PBS containing 0.1% sodium azide and incubated with a rhodamine-labeled goat anti-mouse immunoglobulin M (Chemicon, CA) for 1 h on ice. After two washes with sodium azide-containing PBS, the cells were resuspended in PBS. The GFP- and WSN HA-expressing cells were counted with a FACSCalibur cytometer (Becton Dickinson) according to standard procedures.

To detect WSN NP-positive cells, infected MDCK cells were treated with FACS Permeabilizing Solution (Becton Dickinson) for 10 min at room temperature and then incubated in PBS containing 1% BSA and 0.1% sodium azide. After incubation with an anti-NP monoclonal antibody (2S70/9) and rhodamine-labeled goat anti-mouse immunoglobulin G (Chemicon, CA), WSN NP-expressing cells were detected with the FACSCalibur cytometer. The anti-NP mouse monoclonal antibody (2S70/9) reacts with the NP protein of WSN virus, but not that of the helper PR8 virus (unpublished data).

Quantitative analysis of vRNAs in plasmid-transfected 293T cells. To ascertain the amounts of mutant vRNAs transcribed from the Pol I plasmids in transfected cells, 293T cells were transfected with a plasmid for the transcription of a test vRNA, a plasmid for the transcription of an NS vRNA that is deficient in NS2 synthesis (32), plasmids for the transcription of the remaining six vRNAs, and protein expression plasmids for PB2, PB1, PA, and NP. The plasmid for the expression of a nonfunctional NS2 protein was used to prevent the production of virus capable of undergoing multiple cycles of replication. At 48 h posttransfection, total RNA was extracted with an RNeasy minikit (QIAGEN). To eliminate any residual transfected plasmid DNA, total RNA was treated with an RNase-Free DNase Set (QIAGEN) according to the manufacturer's instructions. The mutant vRNAs were reverse transcribed using TaqMan reverse transcription reagents (Applied Biosystems) with a strand-specific primer (available upon request) for the vRNA and then quantified using the ABI PRISM 7000 sequence detection system with primers (available upon request), TaqMan probes, and the TaqMan universal PCR master mix (Applied Biosystems).

RESULTS

A system to determine the virion incorporation efficiencies of PB2, PB1, and PA vRNAs. Most defective RNA segments of influenza A viruses retain 150 to 300 nucleotides corresponding to the 5′ and 3′ ends of the respective gene segment (7, 15, 24, 27), indicating that these 300 to 600 nucleotides likely possess the structural features required for efficient genome packaging. To identify the regions in the PB2, PB1, and PA vRNAs that are critical for vRNA virion incorporation and virion formation, we first generated plasmids in which the GFP gene is flanked by the noncoding regions and portions of the coding regions derived from both termini [PB2(300)GFP(300), PB1(300)GFP(300), and PA(120)GFP(120)] (outlined in Fig. 2, 3, and 4). Transfection of such a plasmid into 293T cells, together with expression plasmids for the PB2, PB1, PA, and NP proteins (minimal components for transcription and replication of vRNAs), resulted in the expression of GFP in cells (data not shown), indicating that the chimeric vRNAs were synthesized by the cellular RNA polymerase I and transcribed into mRNA by the viral proteins produced by the expression plasmids.

To calculate the vRNA virion incorporation efficiencies, the number of virions containing a test vRNA must be compared with the total number of VLPs. The total number of VLPs could be determined by inoculating cells with VLPs and then counting the number of cells expressing a given influenza virus protein. To

PB1 mutant vRNAs	Number of VLPs (/ml)	Number of VLPs possessing GFP vRNA (/ml)	Efficiency of virion incorporation
PB1(300)GFP(300)	93,000	60,800	65.4%
PB1(120)GFP(120)	134,800	84,000	62.3%
PB1(60)GFP(120)	113,600	67,200	59.2%
PB1(30)GFP(120)	58,800	27,400	46.6%
PB1(21)GFP(120)	125,200	78,200	62.5%
PB1(12)GFP(120)	121,000	70,800	58.5%
PB1(0)GFP(120)	34,200	0	0.0%
PB1(120)GFP(60)	55,000	38,000	69.1%
PB1(120)GFP(30)	44,600	23,800	53.4%
PB1(120)GFP(21)	68,000	26,200	38.5%
PB1(120)GFP(12)	26,800	16,200	60.4%
PB1(120)GFP(0)	19,400	0	0.0%
PB1(0)GFP(0)	42,000	400	1.0%
PB1(-)	49,000	-	-

FIG. 3. Schematic diagram of mutant PB1 vRNAs and their efficiencies in virion formation and virion incorporation. Experiments were performed as outlined in the legend to Fig. 2. All mutants are shown in the negative-sense orientation. Each mutant contains the GFP sequence (green bar) flanked by 24 and 43 nucleotides of the 3′ and 5′ noncoding regions, respectively (gray bars), and coding regions of various lengths (black bars). PB1(−) indicates the omission of this vRNA. The results shown are representative data from three independent experiments.

ensure that the number of infectious VLPs determined by this method was not drastically affected by the viral gene product selected as a marker, we determined the number of cells expressing either HA or NP. Because we were testing the incorporation efficiencies of the PB2, PB1, and PA vRNAs, helper virus was needed to provide functional polymerase proteins. To distinguish between the HA and NP proteins expressed from our test VLPs (derived from WSN virus) and those expressed from the helper PR8 virus, we used antibodies that recognize the WSN HA and NP proteins, but not their PR8 virus counterparts.

To establish a system that allows us to assess the number of VLPs generated, we transfected 293T cells with a plasmid for the transcription of a test vRNA (derived from the PB2, PB1, or PA segment), 7 plasmids for the production of the remaining vRNAs, and 10 expression plasmids for the expression of the viral proteins (i.e., PB2, PB1, PA, HA, NP, NA, M1, M2, NS1, and NS2) (Fig. 1). Forty-eight hours later, VLP-containing supernatants derived from transfected cells were mixed with PR8 helper virus and used to infect MDCK cells. Twelve hours postinfection, we determined the number of cells that expressed either HA or NP protein (Table 1). For all three vRNAs, the numbers of HA- or NP-expressing cells differed by less than a factor of 3; for example, using the PB2(300)GFP(300) test vRNA, we detected 240,800 HA-expressing cells versus 353,200 NP-expressing cells. Therefore, for the subsequent experiments, we determined the number of HA-expressing cells as an indicator of the efficiency of infectious virion formation. The incorporation efficiencies of test vRNAs were thus calculated by dividing the number of GFP-expressing cells (as a marker for the test vRNA) by the sum of the number of HA-expressing cells (as a marker for the number of virions) plus the number of GFP-expressing cells.

Sequences in the coding region of the PB2 vRNA affect infectious virion formation and vRNA virion incorporation. To delineate the sequences in the PB2 vRNA that are critical for virion formation and/or vRNA virion incorporation, we generated a series of plasmids for the production of PB2 vRNAs that express GFP and contain portions of the PB2 coding region

PA mutant vRNAs		Number of VLPs (/ml)	Number of VLPs possessing GFP vRNA (/ml)	Efficiency of virion incorporation
	3' 5'			
PA(120)GFP(120)	24 120 GFP 120 58	588,600	337,400	57.3%
PA(60)GFP(120)	60 120	661,000	368,800	55.8%
PA(30)GFP(120)	30 120	777,200	372,600	47.9%
PA(21)GFP(120)	21 120	1,285,600	806,600	62.7%
PA(12)GFP(120)	12 120	1,170,000	563,400	48.2%
PA(0)GFP(120)	120	284,400	70,000	24.6%
PA(120)GFP(60)	120 60	476,200	288,400	60.6%
PA(120)GFP(30)	120 30	734,600	479,000	65.2%
PA(120)GFP(21)	120 21	652,000	310,000	47.5%
PA(120)GFP(12)	120 12	142,000	40,400	28.5%
PA(120)GFP(0)	120	150,000	62,000	41.3%
PA(0)GFP(0)		143,000	8,000	5.6%
PA(-)	None	87,400	-	-

FIG. 4. Schematic diagram of mutant PA vRNAs and their efficiencies in virion formation and virion incorporation. Experiments were performed as outlined in the legend to Fig. 2. All mutants are shown in the negative-sense orientation. Each mutant contains the GFP sequence (green bar) flanked by 24 and 58 nucleotides of the 3′ and 5′ noncoding regions, respectively (gray bars), and coding regions of various lengths (black bars). PA(−) indicates that this vRNA was omitted. The results shown are representative data from six independent experiments.

derived from both termini (Fig. 2), in addition to the noncoding regions of the PB2 vRNA (Fig. 2). The numbers of VLPs and the incorporation efficiencies of the test vRNAs were determined as described above.

First, we evaluated the efficiencies of infectious VLP production. With PB2(300)GFP(300), which contains 300 nucleotides corresponding to the 5′ and 3′ coding regions of the PB2 vRNA, we detected about 2.8×10^6 VLPs per ml (Fig. 2). Stepwise deletion of the coding sequences at the 3′ end of the vRNA (referred to as the 3′ coding region) had only moderate effects on the efficiency of VLP production; PB2(0)GFP(120), which lacks the entire coding region of the 3′ end, yielded about 1×10^6 VLPs/ml. Deletion of the coding sequences at the 5′ end of the vRNA (referred to as the 5′ coding region) [PB2(120)GFP(0)], however, reduced VLP production by 98% of that of PB2(300)GFP(300) and yielded a number of VLPs comparable to that obtained in the absence of the PB2 vRNA [PB2(−)]. This result suggests that sequences in the 5′ coding region of the PB2 vRNA are critical for the efficient generation of infectious virions. Further analysis revealed that 30 nucleotides of the 5′ coding region are critical for this effect [compare the numbers of VLPs for PB2(120)GFP(0) and PB2(120)GFP(30)].

We next focused on the efficiencies of vRNA virion incorporation and found that for PB2(300)GFP(300), 54.7% of the VLPs contained the PB2(300)GFP(300) test vRNA, indicating that the 300 terminal nucleotides at both ends are sufficient for virion incorporation. To achieve the incorporation efficiencies observed for wild-type segments, internal PB2 coding sequences would likely be required. Stepwise deletion of nucleotides in the 3′ coding region of the PB2 vRNA had only moderate effects provided 30 or more nucleotides were retained; the deletion of these remaining 30 nucleotides, however, reduced the virion incorporation efficiency to 29.5% for PB2(0)GFP(120), demonstrating that this region is important for the efficient incorporation of the PB2 vRNA into virions. For PB2 vRNAs that lack a functional packaging sequence in the 3′ coding region, sequences in the 5′ coding region do contribute to virion incorporation, as exemplified by the inability of the PB2(0)GFP(0) test vRNA to be incorporated.

Deletions in the 5′ coding region only, by contrast, had no effect on incorporation efficiencies, as demonstrated by a 75.7%

TABLE 1. Contributions of individual vRNAs to infectious virion production[a]

Mutant vRNA	No. of VLPs (VLPs/ml) detected by counting:	
	WSN HA-expressing cells[b]	WSN NP-expressing cells[b]
PB2(300)GFP(300)	240,800	353,200
PB2(0)GFP(0)	9,400	16,200
PB2(−)[c]	3,800	11,200
PB1(300)GFP(300)	332,000	292,400
PB1(0)GFP(0)	307,200	147,400
PB1(−)[c]	148,800	108,000
PA(120)GFP(120)	71,000	88,600
PA(0)GFP(0)	23,800	33,200
PA(−)[c]	24,800	24,600
HA(468)GFP(513)	NA	64,000
HA(0)GFP(0)	NA	33,600
HA(−)[c]	NA	27,400
NP(300)GFP(300)	36,600	NA
NP(0)GFP(0)	23,000	NA
NP(−)[c]	21,600	NA
NA(183)GFP(157)	21,600	13,600
NA(0)GFP(0)	15,600	21,600
NA(−)[c]	16,000	15,000
M(222)GFP(220)	24,600	44,600
M(0)GFP(0)	4,200	28,600
M(−)[c]	6,600	22,800
NS(150)GFP(150)	659,400	591,000
NS(0)GFP(0)	214,400	195,800
NS(−)[c]	129,000	122,800

[a] A plasmid for the production of a mutant vRNA and those for the remaining seven authentic WSN vRNAs were transfected into 293T cells, along with protein expression plasmids. VLPs produced from the cells were inoculated into MDCK cells, together with a helper PR8 virus. The efficiency of VLP generation can fluctuate due to subtle differences in experimental conditions. However, the tendencies observed in the efficiency of VLP generation among the test constructs are consistent. Therefore, the results shown are representative data from three independent experiments.

[b] The numbers of VLPs were determined by counting the WSN HA- or NP-expressing cells by flow cytometry. NA, not applicable.

[c] The vRNA was omitted; that is, VLPs were generated in the presence of only seven vRNA segments.

incorporation rate for PB2(120)GFP(0). Thus, while the use of this test vRNA produced a very low number of infectious VLPs, the test vRNA was efficiently incorporated into these particles. This finding suggests that sequences in the PB2 vRNA are involved in two biologically distinct processes: efficient infectious virion formation (a function residing in the 5′ coding region) and efficient vRNA incorporation into particles (a function primarily residing in the 3′ coding region).

The differences in packaging efficiencies could reflect differences in transcription levels of the test vRNAs in 293T cells. To exclude this possibility, we examined the levels of PB2(0)GFP(0) and PB2(120)GFP(120) in plasmid-transfected 293T cells using real-time PCR. The amount of PB2(0)GFP(0) vRNA was 52% of that of PB2(120)GFP(120); however, this difference is unlikely to explain the 99% reduction in VLP generation and the abrogation of vRNA virion incorporation.

The coding regions in the PB1 and PA vRNAs are also required for infectious virion formation and incorporation into virions. Next, we carried out similar experiments for the PB1 and PA vRNAs (Fig. 3 and 4). For the PB1 segment, deletion of the 3′ coding region only [PB1(0)GFP(120)], the 5′ coding region only [PB1(120)GFP(0)], or both coding regions [PB1(0)GFP(0)] reduced the efficiencies of virion formation (Fig. 3), suggesting that sequences at both ends of this vRNA are required for efficient infectious virion formation; the 3- to 7-fold drop in efficiency, however, was much more moderate than the 100-fold reduction observed with some of the PB2 vRNA deletion constructs. We observed a similar pattern for the PA test vRNAs (Fig. 4), in which deletion of the 3′ coding region only [PA(0)GFP(120)], deletions in the 5′ coding region that retained 12 or fewer nucleotides [PA(120)GFP(12) and PA(120)GFP (0)], or deletion of both coding regions [PA(0) GFP(0)] affected the efficiencies of virion formation; the effect, however, was less pronounced than that observed with the PB2 vRNA.

With regard to vRNA virion incorporation efficiencies, we found that for the PB1 segment, 12 nucleotides in the 3′ coding region [PB1(12)GFP(120)] and 12 nucleotides in the 5′ coding region [PB1(120)GFP(12)] were sufficient for efficient incorporation of the respective test vRNAs (Fig. 3), while the deletion of these nucleotides [PB1(0)GFP(120)] and [PB1(120)GFP(0)] abrogated the incorporation of the respective vRNAs into virions. Hence, both ends of the vRNA harbor incorporation signals that seem to act independently and that cannot compensate for each other. For the PA segment, the deletion of sequences in either the 3′ or 5′ coding region affected the incorporation efficiencies only moderately (Fig. 4), while the deletion of both noncoding regions [PA(0) GFP(0)] had a significant effect, suggesting that the synergistic functions of the sequences at both ends of the viral RNA are required for efficient virion incorporation.

To exclude the possibility that differences in transcription levels accounted for the reduced efficiencies of virion formation and/or vRNA virion incorporation, we again determined the amounts of selected test vRNA in plasmid-transfected cells. The amount of PB1(0)GFP(0) was 37.8% of that of PB1(120)GFP(120), while the amount of PA(0)GFP(0) was 30.9% of that of PA(120)GFP(120). As was the case with the PB2 vRNA, these differences are unlikely to explain the differences observed in VLP formation and/or vRNA incorporation.

Hierarchy among vRNA segments in their roles in the incorporation of other vRNAs into virions. Our data suggested that the PB2 vRNA is more critical for efficient infectious virion generation than the PB1 or PA vRNA. We therefore speculated that a hierarchy exists in which the PB2 vRNA is critical for the efficient virion incorporation of other vRNAs, while the omission of other segments is tolerable to some extent. To test this possibility, we examined the effects of both ends of the coding regions in all eight vRNAs on infectious virion formation. For each segment, two test vRNAs were used that either lacked the entire coding sequence or contained sequences from both ends of the coding regions that have been shown by us to allow efficient incorporation (Table 1) [the NA, HA, and NS constructs are described in references 11, 12, and 33; M(0)GFP (0) and M(222)GFP(220), M. Ozawa, J. Maeda, and Y. Kawaoka, unpublished data; NP(0)GFP(0) and NP(300)GFP (300), M. Ozawa and Y. Kawaoka, unpublished data]. We also tested infectious virion formation in the absence of each of the eight vRNA segments. The number of infectious VLPs was determined by counting the number of HA- or NP-expressing cells.

For the majority of the segments, the total numbers of virions differed by less than a factor of 2 for the two detection

systems (i.e., detection of HA- or NP-expressing cells), allowing us to reliably detect overall trends for the efficiency of infectious virion formation. Overall, mutant vRNAs lacking the entire coding region reduced the efficiencies of infectious virion formation compared to the respective vRNAs possessing sequences derived from both the 5′ and 3′ coding regions; the noticeable exception was the NA segment when the number of infectious virions was determined by counting NP-positive cells. In addition, for some vRNA segments, the number of VLPs produced with only seven vRNAs was further reduced compared to the number produced with the test vRNAs that lacked the coding region (Table 1). Most importantly, however, the effects on the efficiency of virion formation differed among the different vRNA segments. Omission of the PB2 vRNA resulted in an ~30-fold reduction in VLP production, whereas omission of the other vRNA segments resulted in 1.4- to 5.1-fold reductions. These results provided further proof of a hierarchy among the vRNA segments with respect to the importance of the individual vRNAs for the incorporation of the other vRNA segments.

To study the contributions of the polymerase and NP vRNAs to virion formation, we had to include a helper virus to provide the corresponding proteins. To ensure comparable experimental conditions, we also used helper virus for the experiments involving the HA, NA, M, and NS vRNA segments, although it could have been omitted for these gene segments. To exclude the possibility that the efficiency of virion formation was affected by the helper virus, the efficiencies of virion formation for mutant HA, NA, M, and NS vRNAs were examined in the absence of helper virus. The results were essentially the same as those shown in Table 1 (data not shown). Therefore, the use of helper virus did not affect the results.

DISCUSSION

Here, we demonstrated that sequences in the coding region of the PB2 vRNA segment of WSN have a dramatic effect on the efficiency of infectious virion formation, as measured by HA- and NP-expressing cells. Although deletions in the coding regions of other vRNA segments also affected the efficiencies of infectious virion formation, these effects were much less dramatic. The PB2 vRNA may, therefore, perform a primary role in the incorporation of other vRNAs into virions.

How do the sequences at the ends of the coding regions of vRNAs contribute to the efficiency of infectious virion formation? In this study, the number of infectious virions was determined by counting HA-expressing cells (when testing for vRNAs other than HA) or NP-expressing cells (when testing for vRNAs other than NP); hence, we examined the effect of a test vRNA on the incorporation of HA or NP vRNA into virions. Our results imply that the truncation of a coding region of a vRNA segment reduces the incorporation efficiencies of the other vRNAs; that is, for all eight individual vRNAs, their coding regions may be required for the efficient virion incorporation of the other vRNA segments. Thus, prior to or at the time of genome incorporation into virions, vRNA segments (as a form of vRNPs) may come together. Indeed, electron microscopy of influenza A virus has revealed that budding virions contain eight RNP molecules (25), indicating that the RNPs likely assemble to form a multisegmented macromolecule consisting of eight RNPs. In retroviruses, genomic RNAs always form dimers in mature virions. Two RNA molecules are linked at the dimer initiation site/dimer linkage sequence (4, 13), which overlaps with the packaging signal. This dimerization of RNA is thought to be important for genome incorporation into virions (31). By analogy, the ends of the coding regions in influenza virus RNAs may serve not only as packaging signals, but also as "linkage sites" that facilitate interactions with other vRNAs. Thus, influenza virus vRNA segments may form a multisegmented macromolecule through these linkage sites by direct or indirect interactions with other vRNA segments. The finding that one segment can affect the incorporation of other segments is consistent with this linkage model. The devastating effect on the incorporation of other vRNA segments suggests a critical role for PB2 vRNA in this process and possibly in the formation of the multisegmented macromolecule. Electron microscopic studies revealed structures in which a center "dot," most likely a vRNP complex, is surrounded by seven dots (25). Based on this finding, one might envision a scenario in which the PB2 vRNA occupies the center position around which the other vRNAs assemble; omission of this center piece may have a more significant effect on the formation of the vRNP structures than the omission of any of the other vRNPs. Likewise, the deletion of the 5′ coding region may abrogate the interaction with the other vRNAs and thus the efficient formation of infectious VLPs. Further studies of the hierarchy among vRNA segments are in progress and should increase our understanding of the mechanism of influenza virus genome packaging.

As previously determined for the HA (33), NA (12), and NS (11) segments, our data indicate that the sequences required for efficient virion incorporation of the PB2, PB1, and PA vRNAs reside in the coding regions. Recently, Dos Santos Afonso et al. also showed that both ends of the coding region of PB2 vRNA were needed for efficient incorporation of the PB2 vRNA in infectious virus (6). Preliminary studies for the remaining NP (Ozawa and Kawaoka, unpublished) and M (Ozawa et al., unpublished) segments produced similar results. Thus, for all eight vRNA segments of influenza A viruses, the ends of the coding regions play important roles in vRNA virion incorporation, although the relative contributions of the 3′ and 5′ ends differ among the vRNA segments. For the NS vRNA, we have further shown that segment-specific noncoding regions are also required for efficient virion incorporation (11). This finding may extend to the other vRNA segments. During the preparation of our manuscript, Liang et al. (19) reported that the 5′-terminal coding region of the PB2 vRNA is more important than the 3′-end coding region for virion incorporation, similar to results previously published by Duhaut and Dimmock (8). Although we agree with Liang et al. (19) that the 5′ coding region contributes to this process, we found that the 3′ end of the PB2 vRNA is more important for efficient virion incorporation. This discrepancy may reflect differences in our assay systems; that is, we evaluated virion incorporation of test vRNA segments in the absence of corresponding authentic vRNA segments, whereas Liang et al. (19) assessed the incorporation of their test vRNAs into virions in the presence of the corresponding authentic vRNA. This competition between the test and the authentic vRNAs for virion incorporation may account for the observed differences.

The precise mechanism by which the packaging signals of different vRNA segments affect their incorporation into virions remains unknown. In influenza virus RNAs, the sequences at the 3′- and 5′-terminal noncoding regions are partially complementary and form a corkscrew structure (2, 5, 9, 14, 30). Although the regions that are important for vRNA virion incorporation are not in immediate proximity, the two structures may be close to each other in the vRNP tertiary structure. It may, therefore, be the tertiary structure, formed by both ends of the coding regions, together with segment-specific noncoding regions, that is recognized by viral components and/or host cell factors as part of the requirements for vRNA incorporation into virions.

ACKNOWLEDGMENTS

We thank Susan Watson and Krisna Wells for editing the manuscript and Gabriele Neumann for critical reading of the manuscript.

This work was supported by CREST (Japan Science and Technology Agency) and by grants-in-aid from the Ministries of Education, Culture, Sports, Science, and Technology and of Health, Labor, and Welfare of Japan and by National Institute of Allergy and Infectious Diseases Public Health Service research grants.

REFERENCES

1. **Berkowitz, R., J. Fisher, and S. P. Goff.** 1996. RNA packaging. Curr. Top. Microbiol. Immunol. **214**:177–218.
2. **Catchpole, A. P., L. J. Mingay, E. Fodor, and G. G. Brownlee.** 2003. Alternative base pairs attenuate influenza A virus when introduced into the duplex region of the conserved viral RNA promoter of either the NS or the PA gene. J. Gen. Virol. **84**:507–515.
3. **Chen, W., P. A. Calvo, D. Malide, J. Gibbs, U. Schubert, I. Bacik, S. Basta, R. O'Neill, J. Schickli, P. Palese, P. Henklein, J. R. Bennink, and J. W. Yewdell.** 2001. A novel influenza A virus mitochondrial protein that induces cell death. Nat. Med. **7**:1306–1312.
4. **Coffin, J.** 1984. Genome structure, p. 261–368. *In* R. Weiss, N. Teich, H. Vermus, and J. Coffin (ed.), RNA tumor viruses. Cold Spring Harbor Laboratory Press, Cold Spring Harbor, N.Y.
5. **Desselberger, U., V. R. Racaniello, J. J. Zazra, and P. Palese.** 1980. The 3′ and 5′-terminal sequences of influenza A, B and C virus RNA segments are highly conserved and show partial inverted complementarity. Gene **8**:315–328.
6. **Dos Santos Afonso, E., N. Escriou, I. Leclercq, S. van der Werf, and N. Naffakh.** 2005. The generation of recombinant influenza A viruses expressing a PB2 fusion protein requires the conservation of a packaging signal overlapping the coding and noncoding regions at the 5′ end of the PB2 segment. Virology **341**:34–46.
7. **Duhaut, S. D., and N. J. Dimmock.** 1998. Heterologous protection of mice from a lethal human H1N1 influenza A virus infection by H3N8 equine defective interfering virus: comparison of defective RNA sequences isolated from the DI inoculum and mouse lung. Virology **248**:241–253.
8. **Duhaut, S. D., and N. J. Dimmock.** 2000. Approximately 150 nucleotides from the 5′ end of an influenza A segment 1 defective virion RNA are needed for genome stability during passage of defective virus in infected cells. Virology **275**:278–285.
9. **Flick, R., and G. Hobom.** 1999. Interaction of influenza virus polymerase with viral RNA in the 'corkscrew' conformation. J. Gen. Virol. **80**:2565–2572.
10. **Fosmire, J. A., K. Hwang, and S. Makino.** 1992. Identification and characterization of a coronavirus packaging signal. J. Virol. **66**:3522–3530.
11. **Fujii, K., Y. Fujii, T. Noda, Y. Muramoto, T. Watanabe, A. Takada, H. Goto, T. Horimoto, and Y. Kawaoka.** 2005. Importance of both the coding and the segment-specific noncoding regions of the influenza A virus NS segment for its efficient incorporation into virions. J. Virol. **79**:3766–3774.
12. **Fujii, Y., H. Goto, T. Watanabe, T. Yoshida, and Y. Kawaoka.** 2003. Selective incorporation of influenza virus RNA segments into virions. Proc. Natl. Acad. Sci. USA **100**:2002–2007.
13. **Greatorex, J., and A. Lever.** 1998. Retroviral RNA dimer linkage. J. Gen. Virol. **79**:2877–2882.
14. **Hsu, M. T., J. D. Parvin, S. Gupta, M. Krystal, and P. Palese.** 1987. Genomic RNAs of influenza viruses are held in a circular conformation in virions and in infected cells by a terminal panhandle. Proc. Natl. Acad. Sci. USA **84**:8140–8144.
15. **Jennings, P. A., J. T. Finch, G. Winter, and J. S. Robertson.** 1983. Does the higher order structure of the influenza virus ribonucleoprotein guide sequence rearrangements in influenza viral RNA? Cell **34**:619–627.
16. **Kobasa, D., M. E. Rodgers, K. Wells, and Y. Kawaoka.** 1997. Neuraminidase hemadsorption activity, conserved in avian influenza A viruses, does not influence viral replication in ducks. J. Virol. **71**:6706–6713.
17. **Lamb, R. A., and R. M. Krug.** 2001. Orthomyxoviridae: the viruses and their replication, p. 1487–1531. *In* D. M. Knipe and P. M. Howley (ed.), Fields virology, 4th ed. Lippincott-Raven Publishers, Philadelphia, Pa.
18. **Lever, A., H. Gottlinger, W. Haseltine, and J. Sodroski.** 1989. Identification of a sequence required for efficient packaging of human immunodeficiency virus type 1 RNA into virions. J. Virol. **63**:4085–4087.
19. **Liang, Y., Y. Hong, and T. G. Parslow.** 2005. *cis*-acting packaging signals in the influenza virus PB1, PB2, and PA genomic RNA segments. J. Virol. **79**:10348–10355.
20. **Nayak, D. P., T. M. Chambers, and R. K. Akkina.** 1985. Defective-interfering (DI) RNAs of influenza viruses: origin, structure, expression, and interference. Curr. Top. Microbiol. Immunol. **114**:103–151.
21. **Neumann, G., T. Watanabe, H. Ito, S. Watanabe, H. Goto, P. Gao, M. Hughes, D. R. Perez, R. Donis, E. Hoffmann, G. Hobom, and Y. Kawaoka.** 1999. Generation of influenza A viruses entirely from cloned cDNAs. Proc. Natl. Acad. Sci. USA **96**:9345–9350.
22. **Neumann, G., T. Watanabe, and Y. Kawaoka.** 2000. Plasmid-driven formation of influenza virus-like particles. J. Virol. **74**:547–551.
23. **Niwa, H., K. Yamamura, and J. Miyazaki.** 1991. Efficient selection for high-expression transfectants with a novel eukaryotic vector. Gene **108**:193–199.
24. **Noble, S., and N. J. Dimmock.** 1995. Characterization of putative defective interfering (DI) A/WSN RNAs isolated from the lungs of mice protected from an otherwise lethal respiratory infection with influenza virus A/WSN (H1N1): a subset of the inoculum DI RNAs. Virology **210**:9–19.
25. **Noda, T., H. Sagara, A. Yen, A. Takada, H. Kida, R. H. Cheng, and Y. Kawaoka.** Architecture of ribonucleoprotein complexes in influenza A virus particles. Nature, in press.
26. **Ochman, H., A. S. Gerber, and D. L. Hartl.** 1988. Genetic applications of an inverse polymerase chain reaction. Genetics **120**:621–623.
27. **Odagiri, T., and K. Tobita.** 1990. Mutation in NS2, a nonstructural protein of influenza A virus, extragenically causes aberrant replication and expression of the PA gene and leads to generation of defective interfering particles. Proc. Natl. Acad. Sci. USA **87**:5988–5992.
28. **Parvin, J. D., P. Palese, A. Honda, A. Ishihama, and M. Krystal.** 1989. Promoter analysis of influenza virus RNA polymerase. J. Virol. **63**:5142–5152.
29. **Pollack, J. R., and D. Ganem.** 1993. An RNA stem-loop structure directs hepatitis B virus genomic RNA encapsidation. J. Virol. **67**:3254–3263.
30. **Robertson, J. S.** 1979. 5′ and 3′ terminal nucleotide sequences of the RNA genome segments of influenza virus. Nucleic Acids Res. **6**:3745–3757.
31. **Sakuragi, J., S. Ueda, A. Iwamoto, and T. Shioda.** 2003. Possible role of dimerization in human immunodeficiency virus type 1 genome RNA packaging. J. Virol. **77**:4060–4069.
32. **Watanabe, T., S. Watanabe, G. Neumann, H. Kida, and Y. Kawaoka.** 2002. Immunogenicity and protective efficacy of replication-incompetent influenza virus-like particles. J. Virol. **76**:767–773.
33. **Watanabe, T., S. Watanabe, T. Noda, Y. Fujii, and Y. Kawaoka.** 2003. Exploitation of nucleic acid packaging signals to generate a novel influenza virus-based vector stably expressing two foreign genes. J. Virol. **77**:10575–10583.
34. **Weiss, B., H. Nitschko, I. Ghattas, R. Wright, and S. Schlesinger.** 1989. Evidence for specificity in the encapsidation of Sindbis virus RNAs. J. Virol. **63**:5310–5318.

FULL PAPER *Virology*

Improvement of a Rapid Diagnosis Kit to Detect Either Influenza A or B Virus Infections

Gui-Rong BAI[1)], Yoshihiro SAKODA[1)], Aaron S. MWEENE[1)], Nobuyuki FUJII[2)], Hidetaka MINAKAWA[2)] and Hiroshi KIDA[1)]*

[1)]*Laboratory of Microbiology, Department of Disease Control, Graduate School of Veterinary Medicine, Hokkaido University, Sapporo 060 0818 and* [2)]*Fujirebio Inc., 51. Komiya-cho, Hachioji-shi, Tokyo 192 0031, Japan*

(Received 21 June 2005/Accepted 16 September 2005)

ABSTRACT. To improve the sensitivity of a kit, ESPLINE® INFLUENZA A&B for rapid diagnosis of influenza by detecting influenza A or B virus specific nucleoproteins (NP), the ESPLINE® INFLUENZA A&B-N was developed by using newly established monoclonal antibodies (MAbs) to the respective NP molecule. MAbs FVA2 11 and FrB1 03 recognize the epitope on the amino acid region 59 130aa of the NP molecule of influenza A virus, and that on the region 72 191aa of the NP of influenza B virus, respectively. The new kit detected influenza A and B virus antigens with a detection limit of $10^{2.0}$–$10^{2.7}$ pfu/test, which is 4 1000 times higher than that of the original kit. Importantly, this kit detected each of influenza A viruses of the known hemagglutinin (HA) subtypes (H1-H15) including the H5N1 viruses recently isolated from human and avian sources in Asia. The kit also detected all of the 15 representative influenza B virus strains tested. The ESPLINE® INFLUENZA A&B-N is thus a rapid and highly sensitive and specific kit for the diagnosis of either influenza A or B virus infections.

KEY WORDS: influenza, monoclonal antibody, rapid diagnosis, sensitivity.

J. Vet. Med. Sci. 68(1): 35 40, 2006

Influenza A viruses infect humans and other mammals and birds, whereas influenza B viruses exclusively infect humans with an exception of infections of seals [12]. All of the influenza A virus hemagglutinin (HA) subtypes H1-H15 [16] and possibly H16 [4] are circulating in aquatic birds, especially in migratory ducks in nature. It has been shown that pigs are susceptible to influenza A viruses of each of the known HA subtypes and the generation of genetic reassortants in the cells lining the upper respiratory tract of pigs upon concurrent infection with influenza virus strains of avian and mammalian origin is an indication that avian viruses of any HA subtype could contribute genes in the production of reassortants [9]. It is, therefore, evident that each virus of the known HA and neuraminidase (NA) subtypes has the potential to provide genes to the virus which may cause future pandemics. In addition, direct transmission of H5N1 avian influenza A viruses to humans in 1997 and during 2003 2005, and H9N2 in 1999 in Asia, as well as another one caused by H7N7 influenza virus in the Netherlands, signaled the necessity to have information on the epidemiology of avian influenza worldwide [3, 10, 13].

The rapid and specific detection of influenza viruses is of significant importance in influenza monitoring and control programs as well as in patient management. The rapid tests for the detection of influenza viruses can easily be used in health care offices or small laboratories that lack complex diagnostic capabilities [1, 2]. In addition, differentiation of influenza A and B viruses may provide health care takers with valuable information regarding possible treatment and prophylaxis. Early detection of infection is of cardinal importance since anti-influenza virus medications are most effective when they are given in the first two days of the onset of symptoms [7]. The influenza virus NP antigen detection kit, ESPLINE® INFLUENZA A&B, has been shown to be specific and widely used for the rapid diagnosis of influenza A and B viruses. To improve its sensitivity, newly established monoclonal antibodies (MAbs) were used to develop the ESPLINE® INFLUENZA A&B-N. In the present study, we evaluated the new kit for the detection of influenza A and B viruses and demonstrated that the sensitivity had improved by 4 1000 times higher than that of the original one.

* CORRESPONDENCE TO: Prof. KIDA, H., Laboratory of Microbiology, Department of Disease Control, Graduate School of Veterinary Medicine, Hokkaido University, Sapporo 060 0818, Japan.

MATERIALS AND METHODS

Cells: Madin-Darby canine kidney (MDCK) cells were grown in Eagle's minimum essential medium (MEM) (Nissui Pharmaceutical Co., Ltd., Japan) supplemented with 10% bovine serum.

Viruses: In the present study, 37 human, 19 equine, 8 swine, one seal, and 43 avian influenza A virus strains, and 15 influenza B virus strains were used.

The human influenza A virus strains were A/PR/8/34 (H1N1), A/New Jersey/8/76 (H1N1), A/USSR/92/77 (H1N1), A/Brazil/11/78 (H1N1), A/Chile/1/83 (H1N1), A/Taiwan/1/86 (H1N1), A/Texas/36/91 (H1N1), A/Beijing/262/95 (H1N1), A/Johannesburg/82/96 (H1N1), A/New Caledonia/20/99 (H1N1), A/Hokkaido/11/02 (H1N1), A/Singapore/1/57 (H2N2), A/Adachi/2/57 (H2N2), A/Aichi/2/68 (H3N2), A/Port Chalmers/1/73 (H3N2), A/Texas/1/77 (H3N2), A/Bangkok/1/79 (H3N2), A/Philippines/2/82 (H3N2), A/Mississippi/1/85 (H3N2), A/Leningrad/360/86

(H3N2), A/Sichuan/2/87 (H3N2), A/England/427/88 (H3N2), A/OMS/5389/88 (H3N2), A/Shanghai/16/89 (H3N2), A/Guizhou/54/89 (H3N2), A/Shanghai/24/90 (H3N2), A/Beijing/32/92 (H3N2), A/Shandong/9/93 (H3N2), A/Kitakyushu/159/93 (H3N2), A/Johannesburg/33/94 (H3N2), A/Sydney/5/97 (H3N2), A/Panama/2007/99 (H3N2), A/Hokkaido/1/03 (H3N2), A/Bangkok/157/03 (H3N2), A/Chanthaburi/230/03 (H3N2), A/Hong Kong/156/97 (H5N1), and A/Hong Kong/483/97 (H5N1).

The equine influenza virus strains were A/equine/Miami/1/63 (H3N8), A/equine/Tokyo/2/71 (H3N8), A/equine/Kentucky/1/81 (H3N8), A/equine/Suffolk/89 (H3N8), A/equine/Alaska/1/91 (H3N8), A/equine/Kentucky/1/91 (H3N8), A/equine/Rome/5/91 (H3N8), A/equine/Taby/91 (H3N8), A/equine/Hong Kong/92 (H3N8), A/equine/Lambourn/22778/92 (H3N8), A/equine/Avesta/1/93 (H3N8), A/equine/La Plata/1/93 (H3N8), A/equine/Newmarket/1/93 (H3N8), A/equine/Newmarket/2/93 (H3N8), A/equine/Kentucky/1/94 (H3N8), A/equine/La Plata/1/95 (H3N8), A/equine/La Plata/1/96 (H3N8), A/equine/Prague/1/56 (H7N7), and A/equine/Newmarket/1/77 (H7N7).

The swine virus strains were A/swine/Iowa/15/30 (H1N1), A/swine/Niigata/1/77 (H1N1), A/swine/Miyagi/3/03 (H1N2), A/swine/Miyagi/5/03 (H1N2), A/swine/Miyagi/7/03 (H1N2), A/swine/Hong Kong/81/78 (H3N2), A/swine/Hong Kong/126/82 (H3N2), and A/swine/Hong Kong/10/98 (H9N2).

The seal virus strain was A/seal/Massachusetts/1/80 (H7N7).

The avian influenza virus strains were A/duck/Mongolia/116/02 (H1N1), A/duck/Mongolia/253/03 (H1N1), A/duck/Hokkaido/17/01 (H2N3), A/duck/Mongolia/174/03 (H2N3), A/duck/Hong Kong/347/78 (H3N1), A/duck/Hokkaido/28/03 (H3N8), A/duck/Czechoslovakia/56 (H4N6), A/duck/Mongolia/107/03 (H4N6), A/chicken/Yamaguchi/7/04 (H5N1), A/chicken/Thailand/142 5/04 (H5N1), A/chicken/Thailand/144 47/04 (H5N1), A/chicken/Thailand/144 54/04 (H5N1), A/chicken/Thailand/144 99/04 (H5N1), A/chicken/Thailand/152 1/04 (H5N1), A/chicken/Suphanburi/1/04 (H5N1), A/duck/Angthong/71/04 (H5N1), A/quail/Angthong/72/04 (H5N1), A/crow/Osaka/102/04 (H5N1), A/duck/Pennsylvania/10128/84 (H5N2), A/duck/Mongolia/54/01 (H5N2), A/turkey/Massachusetts/3740/65 (H6N2), A/duck/Hokkaido/108/03 (H6N8), A/duck/Hokkaido/98/04 (H6N8), A/duck/Hokkaido/139/04 (H6N8), A/chicken/Italy/99 (H7N1), A/turkey/England/63 (H7N3), A/chicken/Pakistan/95 (H7N3), A/chicken/Netherlands/03 (H7N7), A/duck/Mongolia/555/02 (H7N7), A/duck/Mongolia/142/03 (H7N7), A/turkey/Ontario/6118/68 (H8N4), A/turkey/Wisconsin/1/66 (H9N2), A/chicken/aq-Y-55/01 (H9N2), A/chicken/Germany/N/49 (H10N7), A/duck/Mongolia/149/03 (H10N5), A/duck/England/56 (H11N6), A/duck/Hokkaido/85/97 (H11N9), A/duck/Alberta/60/76 (H12N5), A/duck/Hokkaido/66/01 (H12N5), A/gull/Maryland/704/77 (H13N6), A/mallard/Astrakhan/263/82 (H14N5), A/duck/Australia/341/83 (H15N8), and A/duck/Hokkaido/W2/04 (H15N8).

The influenza B virus strains were B/Lee/40, B/Hong Kong/8/73, B/Singapore/222/79, B/Norway/1/84, B/Ann Arbort/1/86, B/Beijing/1/87, B/Victoria/2/87, B/Yamagata/16/88, B/Panama/45/90, B/Harbin/7/94, B/Shandong/7/97, B/Yamanashi/166/98, B/Hokkaido/26/99, B/Chanthaburi/218/03, and B/Bangkok/227/03.

These viruses were prepared from the repository of viruses in our laboratory and propagated in MDCK cells or 10-day-old embryonated chicken eggs.

Expression of panels of NP fragments of influenza A and B viruses: The recombinant NP of influenza A virus (A/NP) and its truncated fragments A/NP 1 159aa, A/NP 162 327aa, A/NP 327 498aa, and A/NP 59 130aa, and that of the influenza B virus (B/NP) and the truncated fragments B/NP 1 200aa, B/NP 190 330aa, B/NP 320 560aa, and B/NP 72 191aa were prepared. These truncated proteins were used for the identification of their respective epitopes. The NPs and the fragments were prepared from the NP genes of A/New Calidonia/20/99 (H1N1) and B/Yamanashi/166/98, respectively. The NP gene segments were amplified by reverse transcriptase-polymerase chain reaction (RT-PCR) and digested by proper endonucleases and ligated into the pW6A expression vector [5] produced from pGEX-2T (Amersham Biosciences). The resulting constructs were transformed into *Escherichia coli* competent cells BL21(DE3) (Novagen) for the expression of panels of NPs. The expressed NPs were purified by a DEAE Sepharose Fast Flow System (Amersham Biosciences) according to the instructions of the manufacturer. The flow-through was applied onto a 50%, 30%, and 15% sucrose gradient and centrifuged at 100,000 × g for 15 hr. The fractions were then analysed by SDS-PAGE. The fraction containing the target protein was dialyzed against 5% sucrose solution for 20 hr. The dialyzed fraction was then applied onto 50% and 15% sucrose gradient and centrifuged as above and the resulting purified protein fraction was used as antigen in this study.

Production of MAbs against NPs of influenza A and B viruses: The MAbs against the NPs of influenza A and B viruses were produced as previously described [8]. Briefly, spleen cell donor BALB/c mice were immunized with the respective recombinant NPs of influenza virus strains A/New Caledonia/20/99 (H1N1) or B/Yamanashi/166/98. The recombinant NPs of the respective viruses were used for the screening of the MAbs-producing hybridoma cells by ELISA. The hybridoma cells producing the MAbs were cloned by limiting dilution and the MAbs were purified from the supernatant fluids of the hybridoma cell cultures.

Establishment of ESPLINE® INFLUENZA A&B-N kit: The immunochromatography and enzyme immunoassay kit was established for the rapid simultaneous detection of influenza A and B viruses. In the assay system, MAbs against the NP of influenza A or B viruses were divided into two parts, one for the capture line on the nitrocellulose membrane and the other for labeling with the alkaline phosphatase. The IgG Fc fragments of the MAbs FVA2 11 and FrB1 03 for influenza A and B viruses, respectively, were

removed and only the IgG Fab fragments were used in subsequent experiments. The IgG Fab fragments of the MAbs against the NP of either influenza A or B viruses were labeled with alkaline phosphatase. The anti-alkaline phosphatase antibodies were fixed at the reference line. The substrate BCIP (5-Bromo-4-chloro-3-indolyl-phosphate) that migrated with the activation buffer reacted with the alkaline phosphatase on the nitrocellulose membrane. When a specimen containing the corresponding viral antigen was dropped onto the kit, a sandwich complex was formed at the judgement line and reacted with the substrate. The newly developed ESPLINE® INFLUENZA A&B-N kit indicated influenza A or B positive results when blue lines were formed on the influenza A or B judgement lines, as well as on the control line. The development of the color on the control line only was indicative of negative results for influenza A or B virus antigens.

Determination of the sensitivity of the ESPLINE® INFLUENZA A&B-N kit: The analytical sensitivity was assessed for two human, one seal influenza A and one influenza B virus strains. Serial 10-fold dilutions of each virus were made and each of the dilutions of the samples was inoculated onto the MDCK cell monolayers for plaque assay [14] and concurrently tested by the kit. The analytical sensitivity was the lowest virus titer (pfu/test) detectable by the kit and was expressed as $\log_{10}$ pfu/test.

Western blotting analysis: Western blotting analysis was used for epitope mapping [15]. The fragments of the recombinant NPs of influenza A and B viruses were separated by 12.5% SDS-polyacrylamide gel electrophoresis. Separated proteins were then electrophoretically transferred to a nitrocellulose transfer membrane (Schleicher & Schuell Bioscience, Germany). The membrane was then blocked with 1% non-fat milk and treated with MAbs FVA2 11 and FrB1 03 against NP of influenza A and B viruses, respectively. Finally, the membrane was treated with peroxidase-labelled goat anti-mouse IgG (Dako Cytomation). Signals were detected by using 4-chloro-1-naphthol substrate (Sigma).

RESULTS

Production of MAbs: A total of 45 hybridoma clones secreting MAbs to the NP of influenza A virus and 51 clones to that of influenza B virus were obtained. Upon further screening, two highly reactive and specific IgG1 MAbs, FVA2 11 and FrB1 03 to the recombinant NPs of influenza A and B viruses, respectively, were selected for use in the diagnostic assay. After purification of the MAbs, their IgG Fab fragments were obtained by papain digestion and labeled with alkaline phosphatase.

Detection of different influenza virus strains with ESPLINE® INFLUENZA A&B-N kit: The kit reacted with each of the human influenza A virus strains tested; 11 H1N1, two H2N2, and 22 H3N2 strains, and two H5N1 strains isolated from humans in Hong Kong in 1997, and 15 influenza B virus strains. The kit also reacted with each of avian influenza virus strains of known HA (H1-H15) and NA (N1-N9) subtypes, swine influenza viruses of H1, H3, and H9 subtypes, equine influenza viruses of subtypes H3 and H7, and an H7N7 seal influenza virus. The sensitivity of the kit was assessed with A/PR/8/34 (H1N1), A/Aichi/2/68 (H3N2), A/seal/Massachusetts/1/80 (H7N7), and B/Lee/40 influenza viruses. The serially diluted samples (30 μl) were dropped onto the kit for testing. As shown in Table 1, the detection limit of the new kit was $10^{2.0}$–$10^{2.7}$ pfu/test for influenza A viruses and $10^{2.1}$ pfu/test for influenza B virus, whereas the detection limit of the original kit was $10^{3.1}$–$10^{5.7}$ pfu/test for influenza A viruses and $10^{3.1}$ pfu/test for influenza B virus. The sensitivity of the detection of influenza A and B virus antigens in the improved kit was 4 1000 times higher than that of the original one (Table 1).

Epitope mapping: To map the epitopes recognized by the MAbs on the NP molecule of influenza A virus, a series of influenza NP fragments were produced. Three NP fragments, A/NP full, A/NP 1 159aa, and A/NP 59 130aa gave positive reactions with MAb FVA2 11 in the Western blotting analysis (Fig. 1). On the other hand, no signal was detected with the fragments A/NP 162 327aa or A/NP 327 498aa. These results indicated that an epitope recognized by MAb FVA2 11 existed on the A/NP 59 130aa fragment.

A series of truncations of NP fragments of influenza B virus were also prepared. MAb FrB1-03 reacted with B/NP full, B/NP 1 200aa, and B/NP 72 191aa, but not with B/NP 190 330aa and B/NP 320 560aa fragments of influenza B virus (Fig. 2). These results indicated the presence of an epitope recognized by MAb FrB1-03 on the B/NP 72 191aa fragment.

Table 1. Sensitivity of ESPLINE® INFLUENZA A&B and ESPLINE® INFLUENZA A&B-N kits

Kits	Detection limits for these viruses ($\log_{10}$ pfu/test)			
	PR/8/34 (H1N1)	Aichi/2/68 (H3N2)	Seal/Mass/80 (H7N7)[a]	B/Lee/40
ESPLINE® INFLUENZA A&B	3.9	3.1	5.7	3.1
ESPLINE® INFLUENZA A&B-N	2.0	2.5	2.7	2.1

a) A/seal/Massachusetts/1/80 (H7N7).

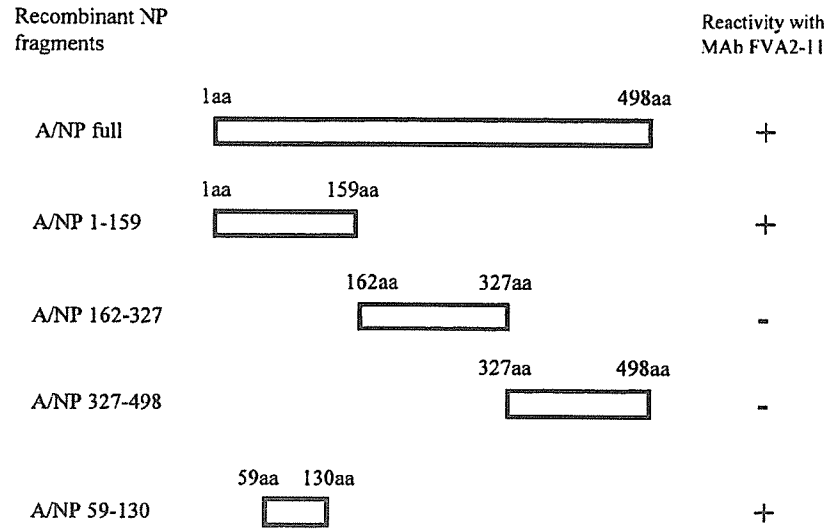

Fig. 1. Determination of the epitope of the FVA2 11 MAb on the NP of influenza A viruses. The Western blotting analysis was used for the determination of the epitope. The A/NP full, A/NP 1 159aa, A/NP 162 327aa, A/NP 327 498aa, and A/NP 59 130aa indicate the lengths of the recombinant NP fragments of the influenza A virus used in this study. The three NP fragments, A/NP full, A/NP 1 159aa, and A/NP 59 130aa gave positive reactions with the MAb FVA2 11. On the other hand, no signal was found with the fragments A/NP 162 327aa or A/NP 327 498aa. The results indicated that the fragment A/NP 59 130 had an epitope recognized by the MAb FVA2 11.

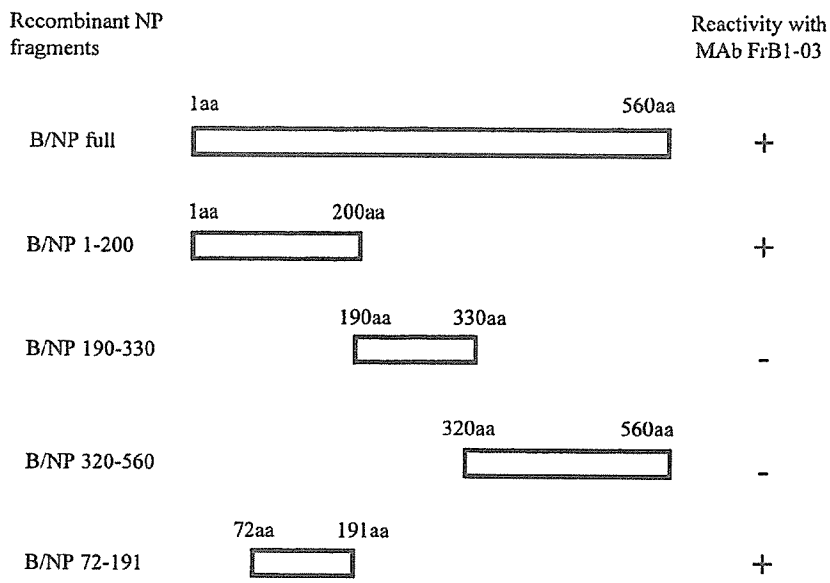

Fig. 2. Determination of the epitope of the FrB1–03 MAb on the NP of influenza B viruses. The B/NP full, B/NP 1 200aa, B/NP 190 330aa, B/NP 320 560aa, and B/NP 72 191aa indicate the lengths of the recombinant NP fragments of the influenza B virus used in this study. The MAb FrB1 03 reacted with B/NP full, B/NP 1 200aa and B/NP 72 191aa but not with the B/NP 190 330aa, and B/NP 320 560aa fragments of the influenza B virus. The results show that the B/NP 72 191aa fragment had an epitope recognized by MAb FrB1 03.

DISCUSSION

In the present study, it has been demonstrated that the ESPLINE® INFLUENZA A&B-N kit is useful for the detection of influenza A and B viruses and can differentiate between them. The reactivity of the kit was assessed on representative human and animal influenza viruses. Each of influenza viruses of human, equine, swine, seal, and avian origin was detected by the kit. The kit is of valuable importance in influenza monitoring and control programmes as it has potential for use in the early detection of influenza outbreaks in humans and animals. All tested influenza A virus strains were detected, indicating that a conserved epitope that is also recognized by MAb FVA2 11 is present in the 37 strains of human and 71 strains of animal influenza A viruses.

Using Western blotting analysis for epitope mapping (Fig. 1), the fragment of the 59 130aa domain of influenza A virus reacted with MAb FVA2 11, whereas, those of the 162 327aa and 327 498aa domains did not. The results indicated that MAb FVA2 11 recognized an epitope on the 59 130aa domain of NP of influenza A viruses. Five hydrophilic regions have been found in the 59 130aa domain by sequence analysis of 66 influenza A viruses (data not shown). The results demonstrated that the domain was highly conserved on the NP molecule in human and animal influenza A virus strains.

In addition, to the use of the newly developed MAbs FVA2 11 and FrB1 03, the labeling of the Fab fragments of the MAbs with alkaline phosphatase may have significantly contributed to the enhancement of the sensitivity of this new kit by 4 1000 times higher than that of the original one. In Table 1, the results of sensitivity were shown only for three subtypes (H1N1, H3N2 and H7N7) of influenza A viruses. Our preliminary investigations demonstrated that the sensitivities of this improved kit for all other influenza A viruses including highly pathogenic H5N1 avian influenza viruses were of the same or higher level than those of the original kit (data not shown). Additionally, no cross-reactivity of the improved kit with a panel of 50 other microorganisms that included 30 respiratory viruses and 20 bacteria was found (data not shown). Further practical study should be necessary to evaluate the usefulness of this new kit for the clinical samples of human and animal influenza.

The detection time is very short since only 15 min are required and performance of the test and interpretation of the results do not require an expert technologist. PCR-based assays offer alternative methods for the diagnosis of influenza virus infections [6, 11]. They potentially have high sensitivity and specificity, but require skill and complex laboratory infrastructure and take several hours to perform. It is concluded that the ESPLINE® INFLUENZA A&B-N is a useful, rapid, reliable, convenient, and simple test for the diagnosis of influenza A and B virus infections in both humans and animals. Clearly, the kit is a valuable addition to the tests already available for the diagnosis of influenza. However, virological examinations including virus isolation should be carried out for the evaluation of the diagnosis by the kit and further characterization of the isolated virus.

ACKNOWLEDGMENTS. We are grateful to Dr. Arunee Chaisingh and Dr. Sujira Parchariyanon, National Institute of Animal Health (Bangkok, Thailand) for the generous provision of the influenza virus isolates of avian species in Thailand. We are also grateful to Dr. Ilaria Capua, Istituto Zooprofilattico Sperimentale delle Venezie (Padova, Italy) generous provision the H7 highly pathogenic avian influenza (HPAI) viruses and to the National Institute of Animal Health (Ibaraki, Japan) for providing the influenza A virus A/chicken/Yamaguchi/7/04 (H5N1). This study was supported by Grants-in-Aid for Scientific Research 15780193 from the Ministry of Education, Culture, Sports, Science, and Technology, Japan.

REFERENCES

1. Barenfanger, J., Drake, C., Leon, N., Mueller, T. and Troutt, T. 2000. Clinical and financial benefits of rapid detection of respiratory viruses: an outcomes study. *J. Clin. Microbiol.* **38**: 2824 2828.
2. Chan, K. H., Maldeis, N., Pope, W., Yup, A., Ozinskas, A., Guill, J., Seto, W. H., Shortridge, K. F. and Peiris, J. S. 2002. Evaluation of the Directigen FluA+B test for rapid diagnosis of influenza virus type A and B infections. *J. Clin. Microbiol.* **40**: 1675 1680.
3. Claas, E. C., Osterhaus, A. D., Van Beek, R., De Jong, J. C., Rimmelzwaan, G. F., Senne, D. A., Krauss, S., Shortridge, K. F. and Webster, R. G. 1998. Human influenza A H5N1 virus related to a highly pathogenic avian influenza virus. *Lancet* **351**: 472 477.
4. Fouchier, R. A., Munster, V., Wallensten, A., Bestebroer, T. M., Herfst, S., Smith, D., Rimmelzwaan, G. F., Olsen, B. and Osterhaus, A. D. 2005. Characterization of a novel influenza A virus hemagglutinin subtype (H16) obtained from black-headed gulls. *J. Virol.* **79**: 2814 2822.
5. Fujimura, K., Ise, N., Ueno, E., Hori, T., Fujii, N. and Okada, M. 1997. Reactivity of recombinant *Treponema pallidum* (r-Tp) antigens with anti-Tp antibodies in human syphilitic sera evaluated by ELISA. *J. Clin. Lab. Anal.* **11**: 315 322.
6. Herrmann, B., Larsson, C. and Zweygberg, B. W. 2001. Simultaneous detection and typing of influenza viruses A and B by a nested reverse transcription-PCR: comparison to virus isolation and antigen detection by immunofluorescence and optical immunoassay (FLU OIA). *J. Clin. Microbiol.* 39: 134 138.
7. Ison, M. G. and Hayden, F. G. 2001. Therapeutic options for the management of influenza. *Curr. Opin. Pharmacol.* **1**: 482 490.
8. Kida, H., Brown, L. E. and Webster, R. G. 1982. Biological activity of monoclonal antibodies to operationally defined antigenic regions on the hemagglutinin molecule of A/Seal/Massachusetts/1/80 (H7N7) influenza virus. *Virology* **122**: 38 47.
9. Kida, H., Ito, T., Yasuda, J., Shimizu, Y., Itakura, C., Shortridge, K. F., Kawaoka, Y. and Webster, R. G. 1994. Potential for transmission of avian influenza viruses to pigs. *J. Gen. Virol.* **75**: 2183 2188.
10. Koopmans, M., Wilbrink, B., Conyn, M., Natrop, G., Van Der Nat, H., Vennema, H., Meijer, A., Van Steenbergen, J., Fouchier, R., Osterhaus, A. and Bosman, A. 2004. Transmission of

H7N7 avian influenza A virus to human beings during a large outbreak in commercial poultry farms in the Netherlands. *Lancet* **363**: 587 593.

11. Moore, C., Hibbitts, S., Owen, N., Corden, S. A., Harrison, G. Fox, J., Gelder, C. and Westmoreland, D. 2004. Development and evaluation of a real-time nucleic acid sequence based amplification assay for rapid detection of influenza A. *J. Med. Virol.* **74**: 619 628.
12. Osterhaus, A. D., Rimmelzwaan, G. F., Martina, B. E., Bestebroer, T. M. and Fouchier, R. A. 2000. Influenza B virus in seals. *Science* **288**: 1051 1053.
13. Peiris, M., Yuen, K. Y., Leung, C. W., Chan, K. H., Ip, P. L., Lai, R. W., Orr, W. K. and Shortridge, K. F. 1999. Human infection with influenza H9N2. *Lancet* **354**: 916 917.
14. Tobita, K. 1975. Permanent canine kidney (MDCK) cells for isolation and plaque assay of influenza B viruses. *Med. Microbiol. Immunol.* **162**: 23 27.
15. Towbin, H., Staehelin, H. and Gordon, J. 1979. Electrophoretic transfer of proteins from polyacrylamide gels to nitrocellulose sheets: procedure and some applications. *Proc. Natl. Acad. Sci. U. S. A.* **76**: 4350 4354.
16. Webster, R. G., Bean, W. J., Gorman, O. T., Chambers, T. M. and Kawaoka, Y. 1992. Evolution and ecology of influenza A viruses. *Microbiol. Rev.* **56**: 152 179.

nature Vol 439|26 January 2006|doi:10.1038/nature04379

LETTERS

Architecture of ribonucleoprotein complexes in influenza A virus particles

Takeshi Noda[1,2,3], Hiroshi Sagara[4], Albert Yen[5], Ayato Takada[3,6]†, Hiroshi Kida[2], R. Holland Cheng[5,7] & Yoshihiro Kawaoka[1,3,6,8]

In viruses, as in eukaryotes, elaborate mechanisms have evolved to protect the genome and to ensure its timely replication and reliable transmission to progeny. Influenza A viruses are enveloped, spherical or filamentous structures, ranging from 80 to 120 nm in diameter[1]. Inside each envelope is a viral genome consisting of eight single-stranded negative-sense RNA segments of 890 to 2,341 nucleotides each[1]. These segments are associated with nucleoprotein and three polymerase subunits, designated PA, PB1 and PB2; the resultant ribonucleoprotein complexes (RNPs) resemble a twisted rod (10–15 nm in width and 30–120 nm in length) that is folded back and coiled on itself[2–4]. Late in viral infection, newly synthesized RNPs are transported from the nucleus to the plasma membrane, where they are incorporated into progeny virions capable of infecting other cells. Here we show, by transmission electron microscopy of serially sectioned virions, that the RNPs of influenza A virus are organized in a distinct pattern (seven segments of different lengths surrounding a central segment). The individual RNPs are suspended from the interior of the viral envelope at the distal end of the budding virion and are oriented perpendicular to the budding tip. This finding argues against random incorporation of RNPs into virions[5], supporting instead a model in which each segment contains specific incorporation signals that enable the RNPs to be recruited and packaged as a complete set[6–12]. A selective mechanism of RNP incorporation into virions and the unique organization of the eight RNP segments may be crucial to maintaining the integrity of the viral genome during repeated cycles of replication.

To elucidate the architecture of the virion interior, we longitudinally and transversely sectioned A/WSN/33 (H1N1) virions budding from Madin–Darby canine kidney (MDCK) cells at 10 h after infection. Although A/WSN/33 virions released into culture medium are spherical in shape[13], the budding virions in longitudinal sections were elongated and contained rod-like structures that were associated with host-derived lipid bilayer envelopes and oriented perpendicular to the budding tip of the virion (Fig. 1a and Supplementary Fig. 1). They were ~12 nm in width and up to 130 nm in length, consistent with the sizes of purified RNPs[2–4]. In transversely sectioned budding virions, electron-dense dots, representing the rod-like structures seen in longitudinal sections, were apparent inside each virion (Fig. 1b). Notably, many of the virions contained eight dots, arranged as seven in a circle surrounding one at the centre (Fig. 1c); not more than eight dots were observed in a virion. To determine the lengths of the rod-like structures, we compared serial transverse sections of whole budding virions (Fig. 1d and Supplementary Fig. 2). In all virions examined, the number of dots decreased progressively with increasing distance from the budding tip of the virion. Together, these results indicate that influenza A virions contain a highly organized set of eight rod-like structures of different lengths (Fig. 2).

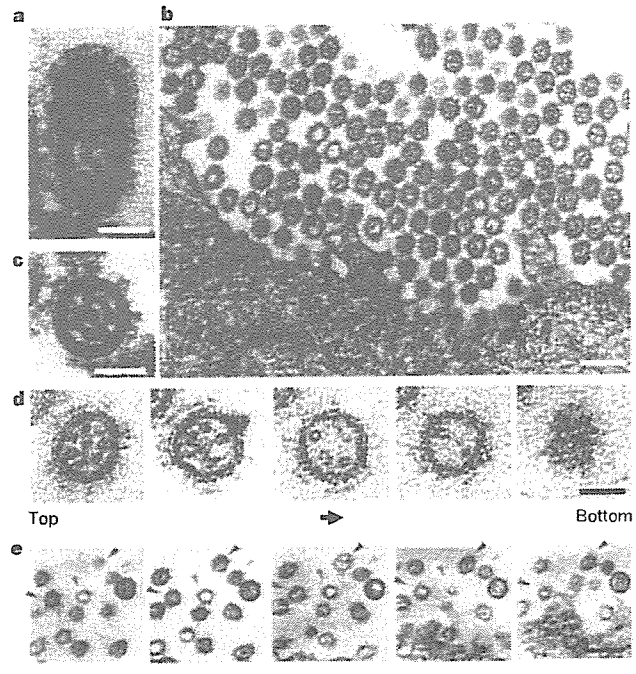

Figure 1 | Budding virions show a specific arrangement of eight rod-like structures of different lengths. a, Rod-like structures, 12 nm in width, are associated with the viral envelope at the distal end of the budding virion. **b**, **c**, Electron-dense dots ($N \leq 8$), representing transversely sectioned rods, were observed in each virion in a characteristic configuration (several peripheral dots surrounding a core dot). **d**, Serial sections of a virion cut from the distal end. As the distance from the end increased the number of dots decreased, suggesting that the eight rod-like structures differed in length. **e**, Lower magnification views of the serial ultrathin sections in **d**, demonstrating that the serial section shown in **d** represents the same virion (circled in red). Other virions are indicated by arrowheads. Scale bars, 50 nm (**a**, **c**, **d**); 200 nm (**b**, **e**).

[1]Internal Research Center for Infectious Diseases, Institute of Medical Science, University of Tokyo, Shirokanedai, Minato-ku, Tokyo 108-8639, Japan. [2]Laboratory of Microbiology, Department of Disease Control, Graduate School of Veterinary Medicine, Hokkaido University, Kita-ku, Sapporo 060-0818, Japan. [3]Core Research for Evolutional Science and Technology, Japan Science and Technology Agency, Kawaguchi, Saitama 332-0012, Japan. [4]Fine Morphology Laboratory, Department of Basic Medical Science, and Division of Virology, Institute of Medical Science, University of Tokyo, Shirokanedai, Minato-ku, Tokyo 108-8639, Japan. [5]Department of Biosciences, Karolinska Institute, 141 57 Huddinge, Sweden. [6]Department of Microbiology and Immunology, Institute of Medical Science, University of Tokyo, Shirokanedai, Minato-ku, Tokyo 108-8639, Japan. [7]Molecular and Cellular Biology, University of California, Davis, California 95616, USA. [8]Department of Pathological Science, School of Veterinary Medicine, University of Wisconsin-Madison, Madison, Wisconsin 53706, USA. †Present address: Research Center for Zoonosis Control, Hokkaido University, Kita-ku, Sapporo 060-0818, Japan.

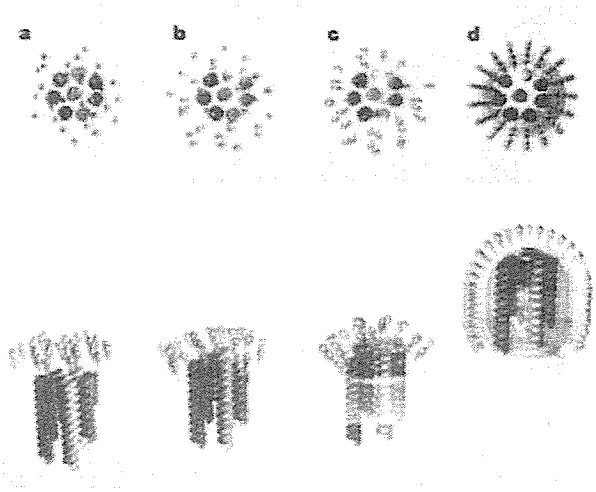

Figure 2 | Rod-like structures in a developing virion. **a–c**, Rod-like structures align vertically with the plasma membrane. **d**, The fully developed budding virion contains a set of eight rod-like structures. Virions in the upper row are viewed from the top; those in the lower row are shown in side profile.

To determine whether or not the arrangement of the virion interior in spherical A/WSN/33 virus is unique to that strain, we examined MDCK cells infected with other strains of spherical influenza A viruses isolated from humans (A/Aichi/2/68 (H3N2) and A/Puerto Rico/8/34 (H1N1)), ducks (A/duck/Hong Kong/836/80 (H3N1) and A/mallard/New York/6750/78 (H2N2)), and swine (A/swine/Chiba/1/91 (H1N2); see Supplementary Fig. 3). In all strains tested, the virions showed the same organization of rod-like structures, in which a central dot was surrounded by seven dots, duplicating the pattern seen in A/WSN/33 virions.

Because some influenza A viruses, especially newly isolated strains, are filamentous[1], we next examined the architecture of the filamentous A/Udorn/307/72 (H3N2) virus. Although most of the transverse sections of filamentous virions lacked electron-dense material (Supplementary Fig. 4a), some showed the typical configuration of seven dots with a single core dot (Supplementary Fig. 4b). In longitudinally sectioned filamentous virions, the rod-like structures were confined to the distal end of each filamentous particle (Supplementary Fig. 4c); the remainder of the virion was empty, consistent with the apparent lack of internal structures in transverse sections of filamentous virions. Thus, both spherical and filamentous influenza virions budding from cells possess an organized set of eight rod-like structures that are associated with the envelope at the budding end of the virion.

Our serendipitous observation that some influenza A virions are partially disrupted when freeze-dried enabled us to study the nature of the rod-like structures inside virions. The widths of the structures released by freeze-dried, negatively stained A/Puerto Rico/8/34 virions were ~12 nm on average (Fig. 3a), similar to the widths of structures inside sectioned virions (Fig. 1). These released structures were morphologically indistinguishable from the RNPs purified from virions in previous studies[2–4] and reacted with anti-nucleoprotein monoclonal antibodies conjugated to colloidal gold (Fig. 3b). To determine further the nature of the rod-like structures observed in virions, we performed ultrathin-section immunoelectron microscopy using mouse monoclonal antibody against nucleoprotein. The electron-dense dots in transversely sectioned virions reacted with anti-nucleoprotein monoclonal antibodies conjugated to gold particles (Fig. 3c), indicating that they were indeed viral RNPs.

To analyse the interior architecture of virions in greater detail, we used electron tomography, which constructs a three-dimensional density map of molecules, the 'tomogram', at a near-molecular resolution[14]. Taking computational thin slices from the map, Fig. 4 shows the results of electron tomography applied to virions budding from MDCK cells. Within a virion, outlined in Fig. 4 by a bilayered membrane with protruding viral glycoproteins, were eight RNPs with a distorted round or square shape. Although some of the RNPs were clearly isolated from each other, there were instances in which peripheral RNPs, as well as central and peripheral RNPs, appeared to be in close contact (Fig. 4, arrows). Whether such contact represents nonspecific association of the RNPs inside the virion or specific interactions with functional significance remains to be determined.

Our findings address a long-standing controversy in influenza virus research: are viral RNA segments incorporated randomly[5] or selectively[6,7] into virions? Together with studies showing that all viral RNPs possess segment-specific packaging signals (refs 8–12; and Y. Muramoto and Y.K., and M. Ozawa and Y.K., unpublished data), our morphological findings clearly favour a model of selective incorporation. Still unclear is how the eight RNPs are organized into a characteristic arrangement within virions. One possibility is that coding regions of the viral RNAs possess signal sequences that promote recruitment of the segments during virion assembly[8], which may then control intersegmental association. Our study contributes

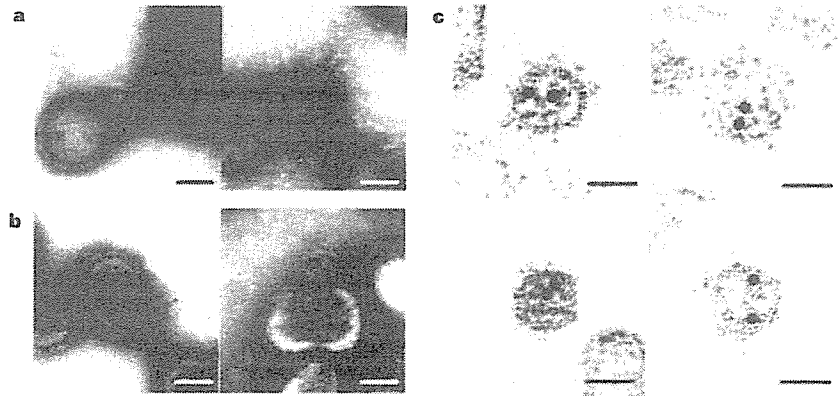

Figure 3 | Identification of rod-like structures in virions as viral RNPs. **a**, Virions ruptured by freeze-drying release twisted rods, 12 nm in width, which are indistinguishable from described purified RNPs[2–4]. **b**, Twisted rods specifically immunolabelled with anti-nucleoprotein monoclonal antibodies conjugated to 5-nm gold particles. **c**, Immunogold labelling of electron-dense dots within transversely sectioned virions with anti-NP monoclonal antibodies conjugated to 10-nm gold particles. Scale bars, 50 nm.

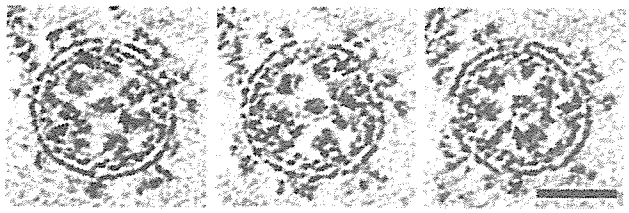

Figure 4 | Electron tomography of RNP complexes in a budding virion. The virion was reconstructed in three dimensions by electron tomography, and three tomograms of its upper portion (at 2.15-nm intervals) containing eight RNPs are shown. Note the close proximities (possible associations) of the RNPs (arrows). Scale bar, 50 nm.

fundamental knowledge to attempts aimed at elucidating the mechanisms of genome incorporation into virions. Defining the interior architecture of influenza virions may speed up the development of both antiviral compounds and more efficient methods of gene delivery and expression.

METHODS

Cells and viruses. A stock of A/WSN/33 (H1N1) was prepared by growing the virus in MDCK cells. Stocks of A/Aichi/2/68 (H3N2), A/Puerto Rico/8/34 (H1N1), A/duck/Hong Kong/836/80 (H3N1), A/mallard/New York/6750/78 (H2N2), A/swine/Chiba/1/91 (H1N2) and A/Udorn/307/72 (H3N2) were prepared in embryonated chicken eggs aged 10–11 d.

Ultrathin section electron microscopy. Electron microscopy was done as described[15]. In brief, MDCK cells were infected with virus at a multiplicity of infection of more than 10 and were then prefixed with 2.5% glutaraldehyde in 0.1 M cacodylate buffer (pH 7.4) on ice for 1 h. After being washed with the same buffer, the cells were post-fixed with 2% osmium tetraoxide on ice for 1 h, stained with uranyl aqueous solution *en bloc*, dehydrated with a series of ethanol gradients followed by propylene oxide treatment, and embedded in Epon 812 Resin mixture. Ultrathin sections (~60-nm thick) were stained with 2% uranyl acetate in 70% ethanol for 3 min at room temperature and in Raynold's lead for 3 min at room temperature, and then examined with a JEM-1200EX electron microscope (Jeol) operated at 80 kV. For ultrathin section-immunoelectron microscopy, the sections were prepared on nickel grids as described above and incubated with saturated sodium periodate solution[16,17], followed by 0.2 M glycine in PBS buffer. After being washed with PBS, the sections were incubated with 1% bovine serum albumin (BSA) in PBS, and then with anti-influenza A virus nucleoprotein mouse monoclonal antibodies. They were then washed with PBS and incubated with a goat anti-mouse immunoglobulin conjugated to 10-nm gold particles (1:100 dilution, BBInternational).

Preparation of serial ultrathin sections. Samples for serial ultrathin sections were prepared as described above. Sections (~20-nm thick) were continuously cut with an Ultracut S ultramicrotome (Leica). The resultant series of ultrathin sections were placed on a single-slot copper grid and examined with an H-7500 electron microscope (Hitachi) operated at 60 kV.

Negative staining of freeze-dried samples. Purified virions were adsorbed to Formvar-carbon-coated copper grids and negatively stained with 2% phosphotungstic acid solution (PTA). Grids were immediately placed in liquid nitrogen and transferred to a JEE-4X vacuum evaporator (Jeol) for freeze-drying. Immunoelectron microscopy was done with freeze-dried samples on nickel grids treated as described above, except that the 2% PTA staining step was omitted. The grids were then treated with 1% BSA in PBS and mouse monoclonal antibodies against influenza A virus nucleoprotein, washed with PBS, and incubated with a goat anti-mouse immunoglobulin conjugated to 5-nm gold particles (1:50 dilution, BBInternational). After being washed, the samples were fixed with 2% glutaraldehyde and negatively stained with 2% PTA.

Tomographic reconstruction. Sections (~50-nm thick) were prepared as described above and affixed to 10-nm colloidal gold particles on the upper surface, which served as fiducial markers for subsequent image alignment. They were then placed in a CompStage specimen holder (FEI) and imaged in a Tecnai G2 Shera (FEI) operating at 200 kV. Images were taken at a magnification of 58,000 every 2° (from −65° to +70°) and recorded by a Gatan CCD camera (1,024 × 1,024 pixels with 0.43 nm per pixel) with an accumulative electron dose of 400 e^{-} A^{-2}. The alignment of the projections was calculated by using IMOD software[18] and the 10-nm gold beads, and the three-dimensional reconstruction was based on an *R*-weighted back projection. Galleries of slice tomograms were displayed with Amira software (Template Graphics) at intervals of 2.15-nm voxels.

Received 26 August; accepted 26 October 2005.

1. Lamb, R. A. & Krug, R. M. in *Fields Virology* (eds Knipe, D. M. & Howley, P. M.) 1487–1532 (Lippincott, Williams & Wilkins, Philadelphia, 2001).
2. Compans, R. W., Content, J. & Duesberg, P. H. Structure of ribonucleoprotein of influenza virus. *J. Virol.* 10, 795–800 (1972).
3. Heggeness, M. H. *et al.* Studies on the helical nucleocapsid of influenza virus. *Virology* 118, 466–470 (1982).
4. Oxford, J. S. & Hockley, D. J. *Orthomyxoviridae. Animal Virus Structure* 213–232 (Elsevier, Amsterdam, 1987).
5. Enami, M., Sharma, G., Benham, C. & Palese, P. An influenza virus containing nine different RNA segments. *Virology* 185, 291–298 (1991).
6. Duhaut, S. D. & McCauley, J. W. Defective RNAs inhibit the assembly of influenza virus genome segments in a segment-specific manner. *Virology* 216, 326–337 (1996).
7. Odagiri, T. & Tashiro, M. Segment-specific noncoding sequences of the influenza virus genome RNA are involved in the specific competition between defective interfering RNA and its progenitor RNA segment at the virion assembly step. *J. Virol.* 71, 2138–2145 (1997).
8. Fujii, Y. *et al.* Selective incorporation of influenza virus RNA segment into virions. *Proc. Natl Acad. Sci. USA* 100, 2002–2007 (2003).
9. Watanabe, T. *et al.* Exploitation of nucleic acid packaging signals to generate a novel influenza virus-based vector stably expressing two foreign genes. *J. Virol.* 77, 10575–10583 (2003).
10. Fujii, K. *et al.* Importance of both the coding and the segment-specific noncoding regions of the influenza A virus NS segment for its efficient incorporation into virions. *J. Virol.* 79, 3766–3774 (2005).
11. Liang, Y., Hong, Y. & Parslow, T. G. *cis*-Acting packaging signals in the influenza virus PB1, PB2, and PA genomic RNA segments. *J. Virol.* 79, 10348–10355 (2005).
12. Dos Santos Afonso, E. *et al.* The generation of recombinant influenza A viruses expressing a PB2 fusion protein requires the conservation of a packaging signal overlapping the coding and noncoding regions at the 5′ end of the PB2 segment. *Virology* 341, 34–46 (2005).
13. Schulze, I. T. The structure of influenza virus. *Virology* 42, 890–904 (1970).
14. Medalia, O. *et al.* Macromolecular architecture in eukaryotic cells visualized by cryoelectron tomography. *Science* 298, 1209–1213 (2002).
15. Noda, T. *et al.* Ebola virus VP40 drives the formation of virus-like filamentous particles along with GP. *J. Virol.* 76, 4855–4865 (2002).
16. Bendayan, M. & Zollinger, M. Ultrastructural localization of antigenic sites on osmium-fixed tissues applying the protein A–gold technique. *J. Histochem. Cytochem.* 31, 101–109 (1983).
17. Bendayan, M. & Maestracci, N. D. Pituitary adenomas: patterns of hPRL and hGH secretion as revealed by high resolution immunocytochemistry. *Biol. Cell* 52, 129–138 (1984).
18. Kremer, J. R., Mastronarde, D. N. & McIntosh, J. R. Computer visualization of three-dimensional image data using IMOD. *J. Struct. Biol.* 116, 71–76 (1996).

Supplementary Information is linked to the online version of the paper at www.nature.com/nature.

Acknowledgements We thank J. Gilbert for editing the manuscript; M. Imai, Y. Muramoto and K. Fujii for discussion; Y. Hirata, K. Aoyama and K. Inoke for technical assistance with electron microscopic tomography; and Y. Kawaoka for illustrations. This work was supported by CREST (Japan Science and Technology Agency), by Grants-in-Aid by the Ministry of Education, Culture, Sports, Science and Technology, by the Ministry of Health, Labor and Welfare, Japan, and by a National Institute of Allergy and Infectious Disease Public Health Service research grant (to Y.K.); and by Swedish Research Council grants and the STINT Foundation (to R.H.C.). T.N. was the recipient of a fellowship from the incorporated foundation SYOUSHISYA and a research fellowship from the Japan Society for the Promotion of Science for Young Scientists.

Author Information Reprints and permissions information is available at npg.nature.com/reprintsandpermissions. The authors declare no competing financial interests. Correspondence and requests for materials should be addressed to Y.K. (Kawaoka@ims.u-tokyo.ac.jp).

Microbiol. Immunol., **50**(1), 73–81, 2006

Editor-Communicated Paper

Highly Pathogenic H5N1 Influenza Virus Causes Coagulopathy in Chickens

Yukiko Muramoto[1,2,3], Hiroichi Ozaki[4], Ayato Takada[5], Chun-Ho Park[6], Yuji Sunden[7], Takashi Umemura[7], Yoshihiro Kawaoka[2,3,8], Haruo Matsuda[9], and Hiroshi Kida*[,1]

[1]Department of Disease Control, Graduate School of Veterinary Medicine, Hokkaido University, Sapporo, Hokkaido 060–0818, Japan, [2]Institute of Medical Science, University of Tokyo, Minato-ku, Tokyo 108–8639, Japan, [3]Core Research for Evolutional Science and Technology, Japan Science and Technology Agency, Kawaguchi, Saitama 332–0012, Japan, [4]Division of Project Research, Creative Research Initiative "Sousei", Hokkaido University, Sapporo, Hokkaido 001–0021, Japan, [5]Department of Global Epidemiology, Research Center for Zoonosis Control, Hokkaido University, Sapporo, Hokkaido 060–0818, Japan, [6]Department of Veterinary Pathology, School of Veterinary Medicine and Animal Sciences, Kitasato University, Towada, Aomori 034–8628, Japan, [7]Department of Veterinary Clinical Science, Graduate School of Veterinary Medicine, Hokkaido University, Sapporo, Hokkaido 060–0818, Japan, [8]Department of Pathobiological Sciences, School of Veterinary Medicine, University of Wisconsin-Madison, Madison, Wisconsin 53706, U.S.A., and [9]Department of Molecular and Applied Bioscience, Graduate School of Biosphere Science, Hiroshima University, Hiroshima, Hiroshima 739–8528, Japan

Communicated by Dr. Kazumasa Ogasawara: Received November 2, 2005. Accepted November 12, 2005

Abstract: **Severe hemorrhage at multiple organs is frequently observed in chickens infected with highly pathogenic avian influenza (HPAI) A viruses. In this study we examined whether HPAI virus infection leads to coagulation disorder in chickens. Pathological examinations showed that the fibrin thrombi were formed in arterioles at the lung, associated with the viral antigens in endothelial cells of chickens infected intravenously with HPAI virus. Hematological analyses of peripheral blood collected from the chickens revealed that coagulopathy was initiated at early stage of infection when viral antigens were detected only in the endothelial cells and monocytes/macrophages. Furthermore, gene expression of the tissue factor, the main initiator of blood coagulation, was upregulated in the spleen, lung, and brain of HPAI virus-infected chickens. These results suggest that dysfunction of endothelial cells and monocytes/macrophages upon HPAI virus infection may induce hemostasis abnormalities represented by the excessive blood coagulation and consumptive coagulopathy in chickens.**

Key words: **H5N1, Avian influenza virus, Blood coagulation**

Influenza A viruses are found in a variety of birds and mammals. Viruses of 16 hemagglutinin (HA) and 9 neuraminidase subtypes have been identified in aquatic birds, the natural reservoir of influenza A viruses (7, 14, 25, 39). These viruses occasionally transmit to other animals and cause disease. Some viruses of particular HA subtypes (H5 and H7) are known to cause highly pathogenic avian influenza (HPAI) in chickens. In comparison with avirulent influenza viruses that induce only local infection in the respiratory or gastrointestinal tracts with subclinical or mild disease (28), HPAI viruses induce lethal systemic infection in chickens. The different pathogenicity of these viruses for chickens is based on the susceptibility of HA to proteolytic cleavage (11, 26). The HPAI viruses have multiple basic amino acids at the cleavage site of HA, which is susceptible for proteolytic activation with ubiquitous endoproteases such as furin (12, 29). Therefore, HPAI viruses are able to infect cells of a broad range of the tissues in chickens, leading to systemic infection with viremia. On the other hand, HA of avirulent influenza viruses has only a single arginine at the cleavage site, which is activated only by trypsin-like proteases at restricted organs, resulting in local infection.

In systemic infection by HPAI viruses, chickens generally show severe depletion, hemorrhages, edema, cutaneous ischemia, and neurological signs and finally

*Address correspondence to Dr. Hiroshi Kida, Department of Disease Control, Graduate School of Veterinary Medicine, Hokkaido University, Kita-18 Nishi-9, Sapporo, Hokkaido 060–0818, Japan. Fax: +81–11–706–5273. E-mail: kida@vetmed.hokudai.ac.jp

die within a few days. Particularly, hemorrhages are observed at multiple organs, for example, lungs, leg shanks and intestines (17, 30, 32). Such severe large hemorrhages imply that HPAI viruses induce blood coagulation disorder to chickens, since blood coagulation plays an important part for the cessation of blood loss from a damaged vessel.

When blood vessel is injured, bleeding initiates the platelet aggregation and the blood coagulation to form the clots. Upon the aggregating of the platelets, the subendothelial coagulation factor named tissue factor initiates extrinsic coagulation cascade by activation of the coagulation factor VII, followed by the activation of the coagulation factors IX, X, VIII, and V, leading to thrombin and fibrin formation, and finally solid clots are generated (16). Tissue factor is constitutively present on the cell membrane of fibroblasts and pericytes in and around blood vessels (18, 20). By contrast, monocytes and endothelial cells contain very little tissue factor activity in normal conditions. But proinflammatory cytokines such as interleukin-1β (IL-1β), tumor necrosis factor-α (TNF-α), and IL-6 induce the expression of tissue factor on those cells (9).

The high frequency of the severe hemorrhage in HPAI virus-infected chickens implies that the blood coagulation disorder is induced. In this study, to examine whether the blood coagulation system is dysregulated upon HPAI virus infection, and if so, to elucidate the possible mechanism to cause the blood coagulation disorder and its implication with the pathogenesis of HPAI virus infection, we compared chickens infected with virulent and avirulent H5N1 viruses pathologically and hematologically.

Materials and Methods

Viruses. Two recombinant influenza viruses, HK156/836 and HK911 were generated by reverse genetics as described previously (33), using avirulent strain A/duck/Hong Kong/836/80 (H3N1) (HK836) as a helper virus. HK156/836 contains HA gene of highly pathogenic A/Hong Kong/156/97 (H5N1) (HK156) and all other genes from HK836. HK911 has the modified HK156 HA gene to express avirulent type of HA and all other genes from HK836 helper virus. Viruses were propagated in the allantoic cavity of 10-day-old embryonated hen's eggs. Virus stocks were stored at −80 C until use. Fifty percent egg infectious dose (EID_{50}) was determined by inoculating serial dilutions of the viruses into eggs, followed by hemagglutination test, using the method of Reed and Muench (24). HK156/836 virus was handled in a biosafety level 3 containment.

Experimental infection of chickens. Six-week-old female specific pathogen-free white leghorn chickens (Nisseiken, Yamanashi, Japan) were infected intravenously with 10^7 EID_{50} of HK156/836 or HK911. After infection, their clinical signs were monitored and blood samples were collected every 6 hr post infection (p.i.) from both chicken groups. The blood samples were treated with sodium citrate (final 0.2%) to prevent clotting and supplied for the examinations of virus titers, thrombocyte counts, and prothrombin times. The virus titers in the blood samples were examined by EID_{50}. All experimental animal studies were undertaken in accordance with the guideline on the Care and Management of Experimental Animals (Japan).

Histopathology and immunohistochemistry. HK156/836-infected chickens were sacrificed at 12 hr post inoculation (p.i.) (2 chickens) and 24 hr p.i. (4 chickens). The comb, lung, bursa, kidney, brain, liver, heart, and spleen were taken from those chickens. Samples from dead chickens were also collected at 18 hr p.i. (1 chicken) and 24 hr p.i. (2 chickens). Collected tissue samples were fixed with 10% formalin solution and embedded in paraffin and sectioned at 4 μm for histological and immunohistochemical examinations. The sections for immunohistological examination were placed on poly-L-lysine coated glass slides. They were deparaffinized, digested by trypsin, and endogenous peroxidase activity was quenched with 3% H_2O_2 in distilled water. After blocking of nonspecific reaction with normal goat serum for 30 min at 37 C, the sections were incubated for 24 hr at 4 C with rabbit anti-strain 499 (H5N3) hyperimmune serum at a 1:2,000 dilution (27). After 5-min wash with phosphate buffered saline (PBS), they were incubated with biotinylated goat anti-IgG antibody (DAKO, Glostrup, Denmark) for 1 hr at 37 C, followed by 5-min wash with PBS and 1 hr incubation at 37 C with peroxidase-conjugated streptavidin (DAKO). Specific reaction was visualized with diaminobenzidine and hydrogen peroxidase.

Counting of thrombocytes in blood samples. The blood samples treated with sodium citrate were smeared on slide glasses and fixed with methanol. The smear samples were stained using anti-chicken thrombocyte monoclonal antibody (HUKT) (13). The numbers of thrombocytes and red blood cells were counted in 20–30 different microscopic fields for each sample and thrombocyte counts are represented as a ratio to red blood cells per ml.

Prothrombin time assay. Prothrombin time of blood samples were measured using a fibrometer (Cobas Fibro, Roche, Basel, Switzerland) and the reagent for the detection of prothrombin time containing 0.5 mg/ml rabbit thromboplastin and 3.0 mg/ml calcium lactate (ThrombocheckPT, Daiichikagaku, Tokyo) according to

manufacturer's protocol. Briefly, after incubation at 37 C for 3 min, 0.1 ml of blood sample was mixed with 0.2 ml of ThrombocheckPT reagent. The time to fibrin-strand formation was monitored with fibrometer.

Semiquantitative reverse transcriptase-polymerase chain reaction (RT-PCR). Chickens infected with HK156/836 or HK911 were sacrificed at 15 hr p.i. and spleens, lungs, and brains were collected. Mock-infected allantoic fluids of the chicken embryo were inoculated into control chickens. Total RNA was extracted from those tissues by Isogen reagents (Nippon Gene, Tokyo) according to manufacturer's instructions. Complementary DNA (cDNA) was synthesized from 600 ng of total RNA using oligo(dT) as a mRNA-specific primer and Moloney murine leukemia virus reverse transcriptase (SuperScript III, Invitrogen, Calif., U.S.A.). cDNA was amplified in PCR thermal cycler using PCR master mix, 2X (Promega, Wis., U.S.A.) with primers specific for chicken tissue factor (GenBank accession no. LOC429084) sense: 5'-GCACTCCGGAATGTAAAG-GAGACCTATACAGCTC-3', antisense: 5'-GCACCGT-GCTTTCTTGACC-3' and GAPDH (22) sense: 5'-GTCTTCACCACCATGGAGAAGGC-3', antisense: 5'-CCAAAGTTGTCATGGATGACCTTGG-3'. The amplification profile for tissue factor involved denaturation at 94 C for 30 sec, annealing at 55 C for 30 sec, and extension at 72 C for 40 sec. And that for GAPDH involved denaturation at 94 C for 30 sec, annealing at 56 C for 30 sec, and extension at 72 C for 30 sec. The reaction cycles of PCR were performed in the range that demonstrated a linear correlation between the amount of cDNA and the yield of PCR products (28 cycles: tissue factor mRNA in lung and brain, 29 cycles: tissue factor mRNA in spleen, and 25 cycles: GAPDH mRNA in lung, brain, and spleen). The PCR products were separated by electrophoresis in 1.5% agarose gels and visualized by ethidium-bromide staining and inspection under UV light. The PCR products were found to be of the expected size, i.e., 430 base pairs for chicken tissue factor and 205 base pairs for chicken GAPDH.

Results

Pathogenicity of Recombinant H5N1 Viruses for Chickens

We prepared two recombinant viruses HK156/836 and HK911 that have different cleavability of HA. HK156/836 has HA from a highly pathogenic strain HK156. HK911 has a modified form of HK156 HA and lacks multiple basic amino acids at the cleavage site (33). All other genes of both recombinant viruses are provided from HK836 strain.

To study pathogenicity of these two viruses, chickens were infected intravenously with 10^7 EID_{50} of HK156/836 or HK911. Chickens infected with HK156/836 showed severe depression peracutely, while HK911-infected chickens did not. Figure 1A shows the survival rates of infected chickens at each time point. One chicken infected with HK156/836 died at 12 hr p.i., and 71% of chickens in this group died within 24 hr p.i. On the other hand, chickens infected with HK911 showed no clinical signs and survived until sacrificed (7 days p.i.). Then, we determined viral titers in the peripheral blood (Fig. 1B). HK156/836 replicated efficiently within 12 hr p.i. and high titers of the virus were detected during the experimental period, while HK911 in the blood was almost undetectable (<10 EID_{50}). These results indicate that HA cleavability is the only factor controlling virus pathogenicity in this experimental system, since these viruses have identical background genes. Thus, these two recombinant viruses with different HA cleavability are a useful model to directly compare the pathogenic events including host responses between virulent and avirulent avian influenza virus infections.

Pathology and Immunohistochemistry of the Chickens Infected with HK156/836

To examine the target organs and the pathologic changes in HK156/836 infection, spleens, lungs, hearts, combs, brains, livers, and kidneys were collected from infected chickens at 12, 18, and 24 hr p.i. and analyzed pathologically and immunohistochemically. At 12 hr p.i., histological changes were not remarkable anywhere except ecchymotic hemorrhage in muscle fascicles of breast in a chicken. Viral antigens were detected in endothelial cells in almost all the organs tested as well as in parenchymal cells in the spleen (Table 1). Notably, these antigen-positive parenchymal cells in the spleen were monocytes/macrophages. In addition, monocytes/macrophages in the peripheral blood were also antigen-positive at 12 hr p.i. At 18 and 24 hr p.i., viral antigens were detected in the parenchymal cells in brains, combs, lungs, and hearts in addition to spleens of the birds. The remarkable degenerative changes were observed in the organs; spleen and bursa had necrosis of lymphocytes with nuclear fragmentation and pyknosis, brain showed the formation of multiple glial nodules with degenerative necrosis of neurons, combs had necrosis with edema and hemorrhages, bursa indicated hemorrhages, and hepatocytes had mild to moderate focal necrosis. Interestingly, fibrin thrombi, consisting of thrombocytes, fibrin, red blood cells, and heterophils, were found in arterioles at lungs in two chickens (No. 7 and 9) (Fig. 2), indicating that blood coagulation was

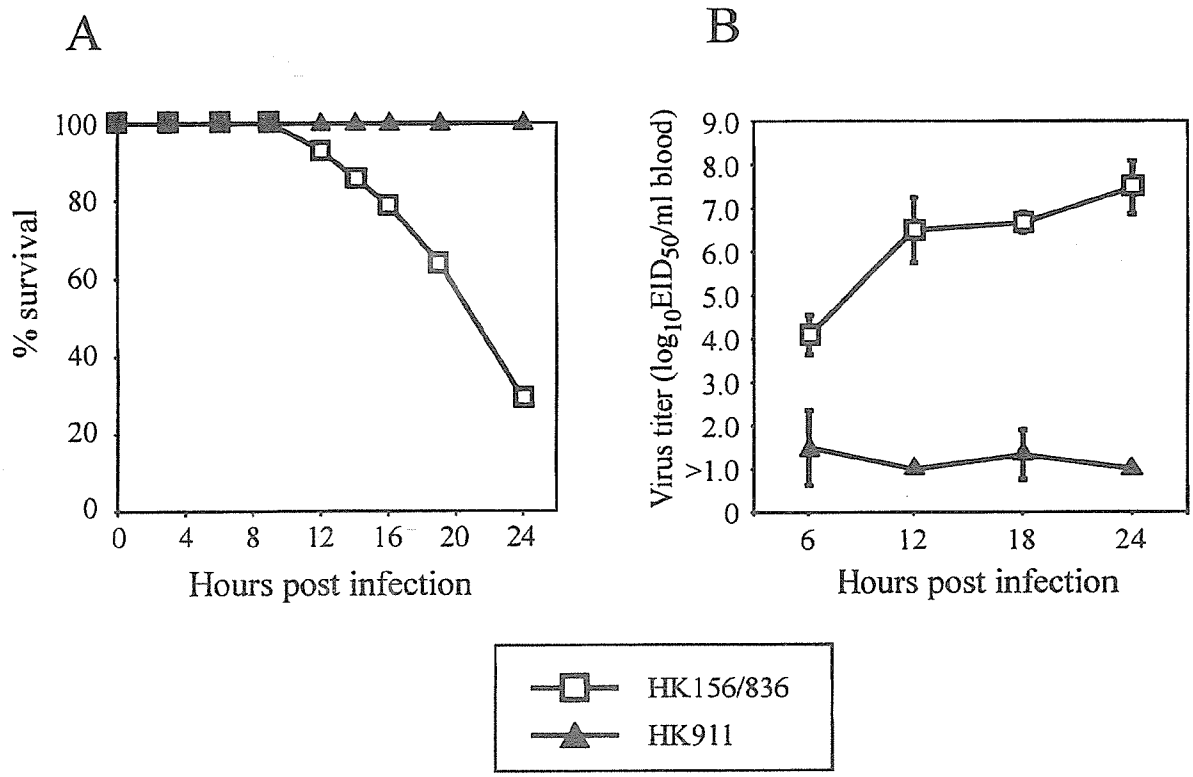

Fig. 1. Comparison of pathogenicity of HK156/836 and HK911 in chickens. (A) Survival rates of virus-infected chickens. Fourteen chickens were infected with HK156/836 intravenously and three chickens were infected with HK911. Chickens were monitored until 24 hr p.i. (B) Virus titers in the peripheral blood of chickens. Blood samples were collected every 6 hr after infection from three chickens infected with HK156/836 or HK911. Virus titers are shown as averages with standard deviations of three chickens of each group.

Table 1. Viral antigens detected in HK156/836-infected chickens in immunohistochemical analysis

Chicken No.	hr p.i.	Spleen		Lung		Heart		Comb		Brain		Liver		Kidney		Monocytes/ macrophages[a]
		E[b]	P[c]	E	P	E	P	E	P	E	P	E	P	E	P	
1	12 sacrificed	+	+	+	−	+	−	+	−	+	−	+	−	−	−	+
2	12 sacrificed	+	+	+	+	+	+	+	−	+	−	+	−	+	−	+
3	18 died	+	+	+	+	+	+	+	+	+	+	+	+	+	−	+
4	24 sacrificed	+	+	+	+	+	+	+	−	+	+	+	−	+	−	+
5	24 sacrificed	+	+	+	+	+	+	+	+	+	+	+	−	+	−	+
6	24 sacrificed	+	+	+	+	+	+	+	+	+	+	+	−	+	−	+
7	24 sacrificed	+	+	+	+	+	+	+	+	+	+	+	−	+	−	+
8	24 died	+	+	+	+	+	+	+	+	+	+	+	−	+	−	+
9	24 died	+	+	+	+	+	+	+	+	+	+	+	−	+	−	+

[a] Monocytes/macrophages in peripheral blood samples.
[b] Endothelial cells.
[c] Parenchymal cells.

initiated in the vessels.

Coagulopathy Induced by HK156/836 Infection

We then examined the numbers of thrombocytes and the prothrombin time of the peripheral blood samples. It is known that thrombocyte is responsible for clot formation and that prothrombin time is an indicator for lack of blood coagulation factors VII, IX, X, prothrombin, or fibrinogen. We collected the peripheral blood from chickens infected with HK156/836 or HK911 every 6 hr sequentially, and counted the number of thrombocytes as described in "Materials and Methods"